AD-A153 466   FATIGUE BEHAVIOR OF UNIDIRECTIONAL FP-AL COMPOSITES   1/1
                WITH CIRCULAR HOLES(U) UTAH UNIV SALT LAKE CITY DEPT OF
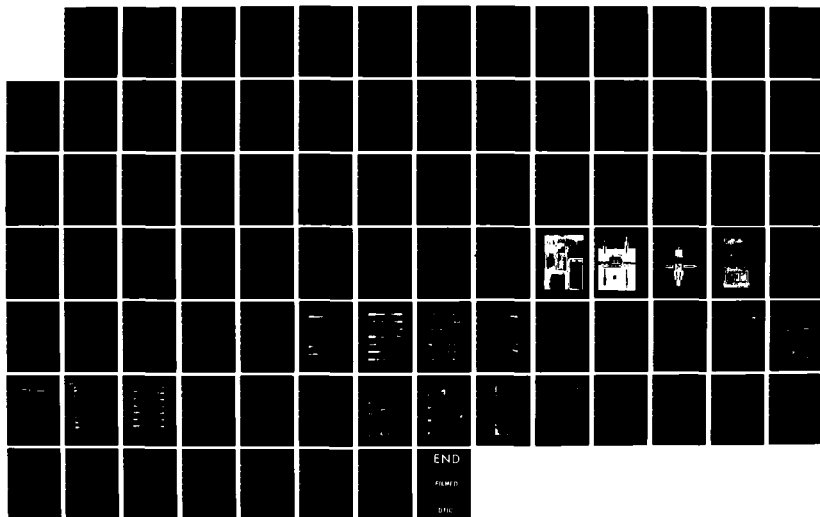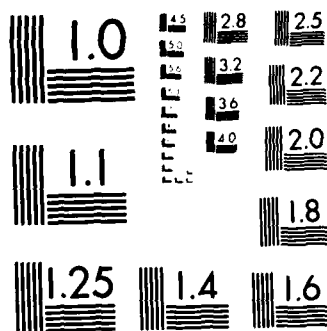   CIVIL ENGINEERING G J DVORAK NOV 84 AMMRC-TR-84-44
UNCLASSIFIED   DAAG46-80-C-0059   F/G 20/11   NL

END
FILMED
DTIC

AD-A153 466

AD

AMMRC TR 84-44

FATIGUE BEHAVIOR OF UNIDIRECTIONAL FP-Al COMPOSITES WITH CIRCULAR HOLES

November 1984

GEORGE J. DVORAK
Department of Civil Engineering
University of Utah
Salt Lake City, Utah 84112

FINAL REPORT   Contract No. DAAG46-80-C-0059

DTIC FILE COPY

APR 2 9 1985

A

Prepared for

ARMY MATERIALS AND MECHANICS RESEARCH CENTER
Watertown, Massachusetts 02172-0001

85   4   246

The findings in this report are not to be construed as an official Department of the Army position, unless so designated by other authorized documents.

Mention of any trade names or manufacturers in this report shall not be construed as advertising nor as an official indorsement or approval of such products or companies by the United States Government.

SECURITY CLASSIFICATION OF THIS PAGE *(When Data Entered)*

REPORT DOCUMENTATION PAGE		READ INSTRUCTIONS BEFORE COMPLETING FORM
1. REPORT NUMBER AMMRC. TR 84-44	**2. GOVT ACCESSION NO.** $\mathcal{A}$ $\mathcal{A}$ 153466	**3. RECIPIENT'S CATALOG NUMBER**
4. TITLE *(and Subtitle)* FATIGUE BEHAVIOR OF UNIDIRECTIONAL FP-Al COMPOSITES WITH CIRCULAR HOLES		**5. TYPE OF REPORT & PERIOD COVERED** Final Report 7/21/80 to 7/20/83
		6. PERFORMING ORG. REPORT NUMBER
7. AUTHOR(s) George J. Dvorak		**8. CONTRACT OR GRANT NUMBER(s)** DAAG46-80-C-0059
9. PERFORMING ORGANIZATION NAME AND ADDRESS Department of Civil Engineering University of Utah Salt Lake City, Utah 84112		**10. PROGRAM ELEMENT, PROJECT, TASK AREA & WORK UNIT NUMBERS** D/A Project: 1L162105AH84
11. CONTROLLING OFFICE NAME AND ADDRESS Army Materials and Mechanics Research Center ATTN: AMXMR-K Watertown, Massachusetts 02172-0001		**12. REPORT DATE** November 1984
		13. NUMBER OF PAGES
14. MONITORING AGENCY NAME & ADDRESS*(if different from Controlling Office)*		**15. SECURITY CLASS. *(of this report)*** Unclassified
		15a. DECLASSIFICATION/DOWNGRADING SCHEDULE

16. DISTRIBUTION STATEMENT *(of this Report)*

Approved for public release; distribution unlimited.

17. DISTRIBUTION STATEMENT *(of the abstract entered in Block 20, if different from Report)*

18. SUPPLEMENTARY NOTES

19. KEY WORDS *(Continue on reverse side if necessary and identify by block number)*

Metal matrix composites	Composite materials
Fiber reinforced composites	Stress concentration
Aluminum	Aluminum oxide fibers
Fatigue	

20. ABSTRACT *(Continue on reverse side if necessary and identify by block number)*

(SEE REVERSE SIDE)

Block No. 20

ABSTRACT

Fatigue behavior of two different batches of fibrous FP-Al composites was investigated. The nominal fiber value fraction of the two batches was 0.52 and 0.55, respectively. Several specimen types were tested: the unnotched coupon, the SL specimen, and two types of coupons with 1/8 in. and 3/8 in. diameter circular holes. One group of unnotched coupons was reinforced in the transverse direction, all other specimens were reinforced in the direction of the applied load.

Cyclic loading was applied at constant amplitude, at three different cyclic ratios R = Smin/Smax, equal to 0.1, -1.0, and -5.0. Certain specimen groups were not tested at R = -1.0 and/or R = -5.0. Endurance limits were evaluated at 2×10^6 cycles of loading. Cyclic load was often applied in 2×10^6 cycle steps, and the load amplitude was elevated after each step, at constant R. Static and residual tension and compression strengths of the test specimens, and elastic properties of the two batches of composite material were also evaluated.

A related analytical investigation of residual thermal stresses, and of the elastic-plastic deformation of the specimens under cyclic loading was performed. The shakedown range of all test specimens was evaluated. Also, local fiber stresses at the circular holes were calculated.

Comparison of experimental and theoretical results suggests that the unnotched SL specimens generally fail at stress amplitudes which are smaller than the calculated shakedown ranges. This seems to suggest that fatigue damage in these specimens is caused by extension of preexisting flaws in the material, which takes place while the matrix experiences elastic cyclic straining. On the other hand, specimens with circular holes fail at stress amplitudes which coincide with, or exceed, the shakedown range. This suggests that fatigue damage may be related to cyclic plastic straining of the matrix.

Fatigue endurance limits are significantly smaller than the residual static strength, especially at R = -1.0, and R = -5.0. The strength reduction is particularly pronounced in compression. The unidirectional FP-Al material delaminates rather easily under compression loading, and this reduces its compression endurance limit to values which can be as low as 9% of the static compression strength.

CONTENTS

1. INTRODUCTION

Material selection in structural design often relies on evaluation of fatigue properties. In the case of fibrous metal matrix composites, such information is available primarily for boron/aluminum and graphite/aluminum systems. However, with the exception of the recent study of Tsangarakis, Slepetz and Nunes (1983), little work has been reported on fatigue behavior of alumina-fiber reinforced aluminum (FP-Al) composites.

This investigation examines the response of the FP-Al system under both tensile and compressive cyclic loads, and also in the presence of circular holes. In the experimental part of the study, fatigue endurance limits have been evaluated at 2×10^6 cycles on unnotched specimens, and on specimens with 1/8 in. and 3/8 in. diameter circular holes. A related analysis of elastic-plastic deformation of the specimens under cyclic loading has been performed and used in interpretation of the experimental data. Of particular interest here was an examination of the relationship between shakedown and onset of fatigue damage in the aluminum matrix, which was demonstrated earlier in experiments on annealed boron-aluminum (Dvorak and Johnson, 1980). Magnitudes of fiber stress in the vicinity of circular holes under cyclic loading were evaluated as well. The fatigue damage modes, under various loading conditions were also examined.

This report describes the experimental program, its results, the plasticity analysis of test specimens, and interpretation of the experimental data.

2. MATERIALS AND SPECIMENS

The FP/Al composite material specimens were obtained from DuPont through AMMRC in two different batches. The first batch was delivered in the summer of 1981, it consisted of unidirectionally reinforced coupons, 6 in. x 0.5 in. x 0.1 in. About 10 of these coupons were reinforced in the direction transverse to the longitudinal specimen axis, and perpendicular to the plate, i.e., the fibers were 0.1 in. long. The remaining 24 coupons of the first batch were reinforced in the longitudinal direction.

The second batch was delivered in the spring of 1983. It consisted of 45 coupons of the 6 in. x 0.5 in. x 0.1 in. size, and of 15 wider coupons, 6 in. x 1.5 in. x 0.1 in. All these coupons were reinforced longitudinally.

The fiber volume fraction of each batch was determined by examination of micrographs taken from sections perpendicular to the fiber direction. Five randomly selected areas were examined at 200x magnification, to determine the number of fibers in a typical area. Also, 400x magnification micrographs were made from these areas to determine the average fiber diameter. The results obtained from this procedure indicated that the nominal fiber folume fraction of the first batch was $c_f = 0.52$, whereas $c_f = 0.55$ for the second batch. The average fiber diameter was equal to 20 µm.

The test specimens made from the available coupons are shown in Figure 1. The shape shown in Figure 1a is the streamlined, or SL specimen designed by Oplinger et al. (1982) for testing of composite materials which are sensitive to failure in the tab or in the gripped area. The streamlined contour makes it possible to avoid this problem by providing a large transition region between the grip and the gage section. Stress

concentrations in this region are significantly reduced, while a uniform axial stress is transmitted in the minimum width section. Although fatigue or static failure of a SL specimen typically takes place at a section which is not identical with the minimum width section, the area of the minimum width section is actually used in calculation of the failure stress.

All SL specimens were machined by an AMMRC supplier. To reduce occasional roughness of machined edges, all specimen edges were smoothed with a fine file and with emery cloth. Also, minimum section dimensions and the position of the longitudinal specimen axis were carefully measured on a magnifying optical bench, and any excentricities detected in this way were compensated for in gripping of the specimens.

All specimens with holes were made from the original coupons at the University of Utah, with carbide or diamond-coated drilling tools.

In addition to the specimens shown in Figure 1, tests were made on 0.5 in. wide coupons without a hole (c.f. Figure 1b). These coupons were used for the transversely reinforced material, and in initial tests of axially reinforced samples. Most of the transversely reinforced specimens failed away from the grip area and thus gave valid results. However, the axially reinforced coupons were sensitive to failure in grip area. Therefore, this design was replaced by the SL specimen, Figure 1a.

All specimen types shown in Figure 1 were used with fiber reinforcement in the longitudinal direction.

3. TEST PROCEDURES

3.1 Instrumentation and Grips

Axial tension and compression testing, both under static and cyclic loading, was conducted on two MTS testing machines of 55 and 165 kip capacity. Axial strain in the specimens was measured by an MTS extensometer, as well as by strain gages mounted on both sides of the specimens. Several specimens were also provided with strain gages for evaluation of both transverse and longitudinal strain. Readout from strain-gage and extensometer measurements was obtained from standard MTS-supplied conditioners and digital voltmeters. These were frequently calibrated with the help of a mechanical extensometer calibration bench.

At the onset of the program, it was anitcipated that all specimens would be tested in standard wedge-type grips. These grips were actually used on all transversely reinforced samples which typically failed in the gage section. On the other hand, the use of the standard grips with the specimens shown in Figure 1 was rejected after some preliminary tests on the following grounds:

a) The FP/Aℓ specimen material was found to be relatively brittle and thus sensitive to geometrical imperfections. Precise specimen alignment in the grips was deemed essential. This could not be achieved in the standard grips.

b) The standard grip assembly with the universal joint would invariably exhibit transverse vibrations during fatigue testing. It was determined that these vibrations were caused by lack of accurate alignment, and also by apparently nonuniform distributions of the fibers, as discussed in more detail below. These vibrations could not be eliminated while standard grips were used.

c)   Both tension and compression tests were contemplated, and this made
     the standard grips unsuitable for the program.

To alleviate these difficulties, two types of custom-made grips were
designed. The first type was a set of bolted flat plate grips with
serrated gripping pads holding the specimen. The side edges of these
grips were carefully aligned and polished. A supporting calibration
table containing two vertical micrometers was made for these grips.
Specimens were fastened in these grips after their precise position was
fixed by the micrometers, on the basis of accurately measured dimensions.
The grips were joined by a temporary bracket before their removal from
the calibration table, to prevent accidental bending of the specimen
during mounting of the grips in the testing machine. Since these flat
plate grips were used only in tension testing, they were attached to the
machine by 1 in. dia. pins. Once the grip specimen assembly was fixed by
the pins, the grips themselves were fastened to auxiliary brackets, sup-
ported on four vertical ground bars by Thompson bearings. These bars were
connected to the frame of the machine in such a way that the brackets and
grips could slide in the direction of applied load, but could not move or
vibrate in the transverse direction. This gripping procedure, although
elaborate and time-consuming, was found to be free of the above-mentioned
problems, and it guaranteed alignment of the specimens with excentricities
not exceeding 0.001 in.

The second type of custom-made grips was designed for testing in
both tension and compression. Figures 2a to 2d show these grips. Figure
2a provides a view of the grips holding a test specimens in the 55 kip
MTS machine. Figure 2b shows a close up of the grip assembly with
lateral micrometers and supporting plattens to prevent specimen buckling.

Figure 2c shows an open disassembled grip, and the tapered ends of the micrometers which are normally in contact with the side edges of the test specimen. Finally, Figure 2d shows a magnified view of the anti-buckling plattens with the rolling pins on the inside. These plattens were loosely fastened to the specimen, with spring-loaded bolts so that the specimen remained free to expand laterally under axial compression load.

Of course, the tension-compression grips are not self-aligning, hence considerable care was required in their manufacture. Their performance was checked with an instrumented steel coupon which was loaded in tension and compression. Normal and transverse, in-plane strains, as well as in-plane and transverse bending strains were measured for the four possible positions of the instrumented coupon in the grips. No measurable excentricity was determined.

The tension-compression grips were used in testing of all SL specimens of the second batch, where compensations had to be made for lateral excentricities caused during machining of specimens. Note that the use of a particular grip is limited to specimens of a constant thickness; this was the case in the present investigation.

An additional advantage derived from the use of the custom-made grips was that specimens required no end tabs. Emery cloth inserts were found sufficient. The required grip clamping force was determined in terms of the torque applied to grip bolts from simple pull-out experiments early in the program, and it was kept approximately constant. The grip bolts were always tightened with an instrumented torque wrench.

3.2 Loading Conditions

All static tests used in determination of elastic moduli and static strengths were conducted at strain rates of the order of 10^{-4}. Slow

cycling was always applied in such measurements to translate the plastic loading surface into the stress range of interest.

The purpose of fatigue tests was to evaluate the endurance limit of each specimen type, for a certain value of $R = S_{min}/S_{max}$, at 2×10^6 cycles. Since specimens were in short supply, it was deemed useful to modify the customary testing prcedure in which a constant stress amplitude is applied to a specimen until failure or runout take place. This procedure requires the use of many specimens as it searches for the endurance limit from above. In the present work the constant stress was applied incrementally, in intervals of 2×10^6 cycles. The first specimens tested in this way were used to identify approximately the endurance limit magnitude. They were usually started at fairly low stress level, and the stress amplitude was gradually elevated, at a constant R, until the specimen failed. Some of these tests took as much as 20×10^6 cycles to complete. Subsequent specimens were first tested at stress levels hich were only slightly lower than the failure stresses of the first samples, and again loaded in 2×10^6 cycle increments until failure.

A concern that immediately arises with this procedure is related to damage development next to the drilled holes. For instance, one may argue that damage growth at lower stress may alleviate the severity of stress concentration without causing failure, and thus strengthen the sample. Other hypothetical situations can be envisioned. The test results do not seem to justify any such concerns as the stress amplitudes at failure showed a remarkably low scatter and were clearly independent of the number of cycles applied to a sample. The modified procedure utilizes almost each specimen to confirm the endurance limit and thus gives rather reliable results from a limited number of samples. Six specimens were

lateral boundary of the hole, at an applied stress approximately equal to the matrix yield stress. Development of plastic zones during loading is illustrated in Figure 31. Upon unloading from plastic state one recovers an elastic domain, about as large as the initial elastic region. Further cycling was conducted to find if the elastic region would expand. This does not actually happen unless one assumes substantial strain hardening in the matrix. Of course, the elastic region on the stress-strain curve translates along the loading axis in a similar manner as in Figure 28.

Stresses in the highly stressed fiber at the boundary of the hole were also evaluated during the loading/unloading cycle. The results are shown in Figure 32. As the matrix yields, the fiber stress grows faster than it would in an elastic specimen.

The results of this loading cycle provide sufficient information for interpretation of the experimental data. Further cycling is possible, but the information found in this way does not seem to justify the cost of additional calculations.

The results obtained for $c_f = 0.52$ are very similar to those one would find for $c_f = 0.55$. If desired, one could make a simple extrapolation. Also, since the specimens shown in Figure 1b and 1c are geometrically similar, the analytical results found for the 0.5 in. wide coupon with a 1/8 in. hole are similar to those one would find for the wider sample with a 3/8 in. hole.

which is an appropriate choice for stress-controlled tests.

With this value of allowable matrix stress, the shakedown range Δ_{sh} of the SL test specimens can be found, from the model in Figure 28. The Young's moduli of the constituents are taken as:

Fiber: $E_f = 380$ GPa

Matrix: $E_m = 72$ GPa, $\sigma_Y = 75$ MPa

The results are:

Shakedown range of SL specimens

c_f	$\dfrac{\Delta_{sh}}{2\sigma_Y^m}$	Δ_{sh} (MPa)
0.52	3.19	478
0.55	3.31	496

In the second column we list the ratio of shakedown range of the composite to the endurance range of the matrix. Note that, from Figure 28:

$$\Delta_{sh}/2\sigma_y^m = E_c/E_m$$

The shakedown limit of the specimens with circular holes, Figure 1, were evaluated with the help of the PAC78 finite element program (Bahei-el-Din, et al., 1981). Figure 29 shows the finite element mesh used in the calculation. Figure 30 shows the calculated stress-strain curve for the specimen, during a single loading cycle, with yield points found for loading and unloading. The matrix yield stress was taken as equal to 10 ksi in this calculation. Initial yielding starts, as expected, at the

Fatigue damage is often observed in the form of matrix fatigue cracking. In composite systems with a relatively weak fiber-matrix bond and large diameter, strong fiber, the cracks tend to propagate around the fibers. Such cracks were found in the annealled B-Aℓ system (Dvorak and Johnson, 1980). They do not damage the fibers, only reduce composite stiffness in proportion to their density. On the other hand, composite systems with strong bonds, and relatively weak, small diameter fibers are often susceptible to fiber breaks caused by the matrix cracks. There, a single matrix crack may break the fibers in its path and extend from the original microscopic size, typically of the order of fiber diameter, to macroscopic or critical size. This process is usually not accompanied by a significant development of distributed cracks and other damage in the matrix, hence no stiffness loss is observed prior to failure. The FP-Aℓ system tested above appears to belong in this latter category, it fails by self-similar crack growth, like a metal or ceramic would under similar circumstances. Additional evidence pointing in this direction was provided by the work of Tsangarakis et al. (1983). Obviously, shakedown analysis may still be useful because it may indicate the loading conditions which should not cause failure in a metal matrix composite which is initially free from damage.

5.2 Shakedown Analysis of Test Specimens

Correlation of fatigue test data with shakedown analysis of composite specimens is best accomplished when the analysis is based on matrix endurance range, rather than yield range (Dvorak and Johnson, 1980). In the present case, the endurance limit of neat matrix material is not known, it can only be estimated from the fatigue tests of transversely reinforced samples. From Table II one finds the value of 75 MPa (11 ksi),

initiated from S_{max}, the σ_m changes from B to C. At C, $\sigma^m = -\sigma_Y^m$ and

compression yielding takes place if S is reduced further. If that happens,

the matrix stress changes along CD, the fiber stress along C'D'. On the

other hand, if $S_{min} < S < S_{max}$ during each cycle, the matrix, and the

composite remain elastic during subsequent cycling. The matrix yield

surface has thus been translated from the original range $-S_Y < S < +S_Y$ to

a new loading range $S_{min} \leq S \leq S_{max}$.

Now, if the loading range is selected in such a way that $S_{max} - S_{min}$

$< 2S_Y$, then the composite will shake down, i.e., assume an elastic deforma-

tion cycle after an initial excursion into the plastic domain. Clearly,

the shakedown range may be shifted on S axis at will, as long as $\sigma^f < \sigma_Y^f$,

the fiber yield or failure stress. It is probably obvious that the

shakedown range magnitude is not influenced in any way by any initial

residual stress which may be present in the composite. Indeed, it would

remain same if the initial state was anywhere in the region AB. Hence

the initial residual stress state caused by fabrication has no influence

on the shakedown condition.

The shakedown phenomenon is of considerable interest in fatigue of

fibrous composite materials, c.f., Dvorak and Johnson (1980). Specifically,

if the composite shakes down, and if the matrix endurance limit (defined

at certain N cycles) is not smaller than the matrix yield stress, then

the matrix does not experience low cycle fatigue. Indeed, it may resist

fatigue damage for the number of cycles for which the matrix endurance

limit was originally defined. Conversely, if the loading amplitude

$S_{max} - S_{min}$ is larger than $2S_Y$, then the composite may not shake down.

The matrix is deformed plastically during each cycle, and it usually

suffers fatigue damage after about 50,000 cycles of loading.

direction of a mutual constraint between matrix and fiber. In fibrous materials the principal constraint exists in the fiber direction, that is also the direction of applied load. Minor constraints exist in other loading directions. Numerous examples of this phenomenon were shown by Dvorak et al. (1975a, 1975b), and Teply (1984).

An illustration appears in Figure 28. We consider the response of a fiber composite represented by a material model consisting of a fiber and a matrix element, both attached to rigid plates at the ends. Here, V_m and V_f indicate phase volume fractions, E_m, E_f the Young's moduli. This model is quite adequate for reasonably accurate examinations of plastic response of a unidirectional composite in uniaxial tension. The macroscopic stress S is applied through the rigid plates as shown. Our objective is to estimate the fiber and matrix stresses σ^f and σ^m in the course of a macroscopic loading cycle S. Without the loss of generality one may assume that the composite is initially stress free.

The response of the composite element under load is shown in Figure 28. The overall stress S is plotted on the horizontal axis, the local axial normal stresses σ^m, σ^f on the vertical axis. Now, when S > 0 is first applied to the element, both fiber and matrix deform elastically, local stresses σ^f, σ^m increase from 0 to A', and A, respectively. At $S = S_Y$ the matrix yield stress is reached, $\sigma^m = \sigma^m_Y$. If the matrix is assumed to be perfectly plastic, then no additional stress increase takes place in the matrix, $\sigma^m = \sigma^m_Y$ at $S \geq S_y$. Of course, matrix hardening can be introduced without difficulty. Now, any additional increment in S is taken up by the fiber, for $S \geq S_Y$ the fiber and matrix stress increments are $d\sigma^f = dS/V_f$, $d\sigma^m \equiv 0$.

Suppose that $S = S_{max}$, and σ^f, σ^m are at B', B. If unloading is

components, at the end of the cooldown cycle at room temperature, is sig-
nificantly affected by the fact that the matrix yields plastically, through
the entire cooldown period. In the case of the FP-Aℓ system fabricated
by vacuum casting, the material deforms in a viscous manner after solidi-
fication, and then plastically. The viscous and inviscid modes are mixed
and their relative contributions depend on the rate of cooling. In any
event, the magnitude of matrix stresses after cooldown is such that the
largest normal stress is found in the fiber direction and is almost equal
to the matrix tension yield strength at room temperature. Thus its magni-
tude is usually equal to 10 ksi or so in aluminum, and it is not strongly
dependent on the thermoelastic constants of the fiber or matrix. The
hoop stress is of similar magnitude, also tensile, the radial stress is
much smaller and it is compressive. Actual values are unimportant, for
as will be seen later, the initial stress state is completely changed by
subsequent cyclic loading.

It follows that the as-fabricated composite when loaded in tension,
deforms plastically from the onset of load application. This has been
observed in the present work, and also by Tsangarakis et al. (1983).
However, if the composite is unloaded after initial loading, it immedi-
ately becomes elastic and deforms elastically until the matrix axial
normal stress reaches the value of compressive yield stress.

In the case of constant amplitude cyclic loading one can select a
load amplitude which keeps the composite entirely in the elastic range,
or, alternatively, a load amplitude which causes plastic straining of the
matrix in a certain part of the cycle.

This behavior is associated with the phenomenon of constraint
hardening, which allows the composite yield surface to translate in the

5. ANALYTICAL RESULTS

5.1 Shakedown and Fatigue in Fibrous Composites

Interpretation of the experimental results reported above can be
facilitated by theoretical analysis of mechanical behavior of test
specimens in the course of fabrication and subsequent monotonic or cyclic
loading. Of course, the dominant feature of mechanical behavior of metal
matrix composites is the plastic deformation of the matrix, which affects
the overall response. Many aspects of composite plasticity have been
described in the work by Dvorak et al. (1975, 1976, 1984), hence we limit
our attention to specific results pertaining to the present experimental
program.

The residual stresses which are present in the fibrous composite
after fabrication can be determined without difficulty, by analyzing the
plastic response during cooldown from the fabrication temperature.
Several techniques can be utilized for this purpose, some have been
described by Dvorak and Rao (1976) and Dvorak and Wung (1984), together
with specific examples for B-Aℓ, W-Cu, and graphite-aluminum systems.
The results obtained for these different systems are remarkably similar
in several respects; and thus provide useful guidance for the case of the
FP-Aℓ system which has thermomechenical properties similar to those of
B-Aℓ. First, thermal expansivity of the aluminum matrix is much larger
than that of the fiber. During cooldown from fabrication temperature the
matrix tends to contract much more than the fiber, and this causes devel-
opment of residual stresses. In general, there is a significant tension
normal stress in the matrix, in the fiber direction. Also, tensile hoop
stress and compressive radial stresses are present in the matrix, in the
vicinity of fiber-matrix interface. The magnitude of these stress

by cycling. All failures were in out-of-plane shear, probably preceded by fiber buckling or kinking.

Results of the last set of tests on 1 1/2 in. wide coupons with a 3/8 in. hole are presented in Tables XII and XIII for R = 0.1, and R = -1.0, respectively. Corresponding graphs are shown in Figures 21 and 22. Broken samples photographs are presented in Figures 23 to 25, and corresponding radiographs in Figures 26 and 27. These specimens showed a strong tendency to delaminate at R = -1. This is evident from Figure 22, and from the photographs in Figures 24, 25, and 27. In fact, delamination was the only mode of fatigue failure in these samples at R = -1. The delaminated specimens were tested in static tension. Compression tests of these samples were not performed because relatively large forces would have been involved and there was concern about possible damage to the antibuckling plattens, and to grips, during sudden specimen failure.

The results of compression static tests, i.e., the residual compression strength should be regarded with caution. Most of the specimens tested at R = -1 and R = -5 delaminated before the test was conducted, and some were held together only by the bolted grips, Figure 2. Such support may not be available in a composite structure where a hole may cause onset of catastrophic delamination failure at compression stresses which are smaller than the values shown in Table II.

with incremental loading, Section 3.2.

Tables VI to VIII present the data for SL specimens tested at R = 0.1, R = -1.0, and R = -5.0. Figures 6 to 8 show these results in graphs. Figures 9 to 11 show the broken specimens. Of particular interest here is the delamination caused by high compressive stress at R = -5, Figure 11. To explore the extent of possibly invisible internal delamination in these SL specimens, radiographs of the broken samples were made. These appear in Figure 12; the specimens are arranged in the same order as those found in Figure 11. A comparison of these two figures suggests that the delaminated zones which appear on the radiograph can also be seen on the photographs. This is generally true for all similar comparisons that follow. The stress level at onset of delamination at R = -5 corresponds to the endurance limit. Specimens were inspected visually for possible delamination after termination of each incremental loading step. The grips provided sufficient support at the specimen ends for the delamination to proceed in the midsection of the specimen. Some of the specimens with incipient delaminations were tested statically.

Tables IX to XI and Figures 13 to 15 present fatigue test results for 0.5 in. wide coupons with a 1/8 in. hole, tested at R = 0.1, R = -1, and R = -5, respectively. Delamination started to appear at R = -1, at the stress levels corresponding to maximum cyclic load applied to the specimen. Delaminations are illustrated in Figures 16-18 which show the broken samples. Also, in Figures 19 and 20, on radiographs of specimens from Figures 17 and 18. Note that the image that appears in Figure 20 has been reversed against that shown in Figure 18.

Three static compression tests were performed on uncycled specimens in this set of experiments. Compression strength appears to be unaffected

The next three columns refer to residual static strength of specimens which survived cyclic loading. The ratio S_n/S_o denotes the residual tensile strength of notched specimens divided by that of the unnotched SL sample tested at a certain R. The last two columns indicate the ratio of endurance limit S^e to static residual strength S. Both values are taken either in tension, or in compression. Note the strong effect of decreasing R on S^e/S, and the remarkably low values of compression S^e/S, caused by delamination of test specimens.

4.2.2   Batch No. 1, $c_f = 0.52$

Detailed description of test results obtained on this material will now be presented.

Table III and Figure 3 show the results for transversely reinforced 0.5 wide coupons. The standard testing procedure was followed here, not the incremental one discussed in Section 3.2.

Table IV and Figure 4 show test results for longitudinally reinforced SL specimens. The incremental loading technique of Section 3.2 was used. The results are thus plotted in Figure 4 on a linear cycle scale, rather than the usual logarithmic scale. In this and later figures a dark circle denotes failure, an open circle indicates runout followed by a static test for residual strength.

Table V and Figure 5 give results for longitudinally reinforced coupons with a drilled 1/8 in. hole. Again, the incremental loading technique was used.

4.2.3   Batch No. 2, $c_f = 0.55$

All samples in this batch were reinforced with fibers parallel to the longitudinal direction. Also, all tests in this group were conducted

such test was there a measurable reduction of the modulus that could be attributed to damage growth in the cycled sample.

4.2 Fatigue Test Results

4.2.1 Summary of Results

As pointed out in Section 3.2, the purpose of fatigue testing was to evaluate the endurance limit of a given specimen set at 2×10^6 cycles of loading applied at a constant value of the cyclic stress ratio R. In addition, residual static strength in tension, or in compression, was determined on selected specimens. Also, the stress level at which delamination of specimen material was first observed was recorded.

Prior to proceeding with the detailed description of individual test results, we present a summary of all results in Table II.

The first column gives the nominal fiber volume fraction of the specimen material. Recall that $c_f = 0.52$ refers to the first batch of samples delivered in 1981, while $c_f = 0.55$ denotes the second batch received in 1983. Specimen types are shown in Figure 1, the transversely reinforced coupon had the dimensions shown in Figure 1b, without the hole. The third column lists the cyclic stress ratio $R = S_{min}/S_{max}$. Measured endurance limits S^e are listed in the fourth column. Next we show the endurance range $\Delta^e = S_{max}^e - S_{min}^e$. The sixth column indicates the ratios of notched fatigue strength S_n^e to the unnotched value S_o^e found for the SL specimen at a certain value of R. The seventh column gives similar ratio for the endurance range Δ_n^e/Δ_o^e. Note that with decreasing R the ratio S_n^e/S_o^e decreases, so does Δ_n^e/Δ_o^e, but at somewhat different rate. Also, the compression stress component at $R < 0$ reduces tensile fatigue strength but the total stress range expands in the direction of compressive stress.

This provides an indication that the coupons are not necessarily homogeneous in the transverse direction, probably as a consequence of uneven fiber distribution in the transverse plane, or due to internal damage, or both. In any event, the above results were utilized in sorting of the specimens for fatigue testing. Specimens with largest excentricity Δ were tested only in tension. Those with moderate Δ were selected for tension-compression tests at $R = -1$ ($R = S_{min}/S_{max}$), and those with low Δ for tests at $R = -5$.

In addition to the moduli, static strength and strain to failure were measured on selected specimens. All static test results appear in Table I.

TABLE I   Static Test Results

Batch	E (GPa)	ν	U.T.S. (MPa)	ε_f (%)
1 (Transverse)	143		171	0.37
1 (Axial)	216	0.27	581	0.30
2 (Axial)	228	0.25	600	0.32

It should be emphasized that the ultimate tensile strength and failure strain were obtained on one or two specimens. This was done to save as many specimens as possible for fatigue testing; static strength data are generally available in the literature. Therefore, the above U.T.S. and ε_f values should be regarded as approximate, and more attention should be given to the residual strength values of fatigue tested specimens which are reported in the sequel.

Overall Young's moduli were also measured on specimens with and without holes which were previously subjected to fatigue loading. In no

4. TEST RESULTS

4.1 <u>Elastic Moduli and Static Strength</u>

Young's modulus and Poisson's ratio of the specimen material were measured on prismatic coupons, in as-delivered state, before these coupons were made into SL or other specimens shown in Figure 1. In the case of the specimens of the first batch, strain was measured by strain gages bonded to the specimen surface, and the stress-strain curve was plotted on an x-y recorder. Each specimen was loaded in several cycles. Plastic straining was frequently observed during loading, while elastic behavior was evident during unloading. The unloading elastic modulus was taken as equal to the Young's modulus.

Specimens of the second batch were examined in a different way. An extensometer was attached first to one, and then to the other specimen surface. In each configuration the unloading elastic modulus was measured during each of six unloading cycles. The strain in this case was read directly on the digital display, together with the applied stress. Average moduli for each configuration were calculated and compared as follows: Let E_A, E_B be the Young's moduli measured on either side of the specimen such that $E_A > E_B$. Furthermore, let $\Delta = (E_A - E_B)/E_A$. On 41 coupons examined, it was found that $0 < \Delta < 0.038$ with the following distribution:

No. of Specimens	100 Δ	No. of Specimens	100 Δ
13	0 ÷ 0.5	2	2.0 ÷ 2.5
6	0.5 ÷ 1.0	4	2.5 ÷ 3.0
6	1.0 ÷ 1.5	2	3.0 ÷ 3.5
6	1.5 ÷ 2.0	2	3.5 ÷ 4.0

typically used to establish the endurance limit, where twice as many would be needed if the standard procedure was followed.

An additional advantage of the modified procedure became evident in the course of tension-compression cyclic testing. Fatigue failure was often preceded by longitudinal delamination which started at the drilled holes, or in the narrow section of SL specimens. The incremental loading technique made it possible to detect the stress level at which delamination had first appeared.

6. INTERPRETATION OF EXPERIMENTAL RESULTS

The analytical results of the previous sections provide a certain insight into the internal stresses in the test specimens, and into their changes during cyclic loading. However, it must be pointed out that very little is known about actual in-situ properties of the aluminum-lithium matrix. Our attempts to obtain the matrix material were not successful. This makes it difficult to evaluate the quantities of interest with a desirable degree of accuracy. Hence, the analytical results must be compared with experiments only in regard to obvious trends, less emphasis should be placed on specific numerical values.

First, consider the connection between shakedown and onset of fatigue damage. If there was a definite connection, then no sample would fail below its shakedown limit, or within its shakedown range. It may only fail outside this range. When this proposition is examined for the SL specimens, one finds from table on p. 20 that the shakedown range Δ_{sh} is equal to 478 MPa at $c_f = 0.52$, and to 496 MPa at $c_f = 0.55$. In contrast, corresponding experimental results in Table IV show that the endurance range of SL specimens was equal to only 366 MPa at $c_f = 0.52$, $R = 0.1$, and to 409 MPa at $c_f = 0.55$, $R = 0.1$. In both instances failure took place well within the calculated shakedown range. On the other hand, at $R = -1.0$ in $c_f = 0.55$ material, the endurance range agrees with the shakedown range, and exceeds it by almost a factor of two at $R = -5$.

One may ask if the tension-tension specimens did fail because of high fiber stresses. This question is difficult to answer because the fiber fatigue strength is not known. Clearly, the static fiber strength was not exceeded at endurance limit.

Thus the reasons for fatigue failure at $R = 0.1$ are not to be

derived from the above-mentioned possibility of matrix damage caused by cyclic plastic straining. The samples fail well within the elastic range. A more feasible explanation is that the failure was caused by propagation of internal flaws which were present in the material after fabrication. Also, hidden surface damage caused by machining of the samples may be responsible. We recall that rather extensive areas of dry fibers, and many broken fibers were found in the FP-Aℓ material by Tsangarakis et al. (1983). We note that the material of our first batch is from the same melt as batch no. 1 in Tsangarakis et al. (1983). As expected, identical values were found in their and our investigation for identical quantities.

Next, the question about shakedown and fatigue can be posed for the specimens with holes: Can one relate the shakedown and endurance ranges? An affirmative answer can be given in this case. From Figures 30 one can find that the shakedown range for the specimen is of approximately same magnitude as the shakedown range of the matrix. For $c_f = 0.52$ one finds that the matrix shakedown range is equal approximately to 150 MPA (2 x 75 MPa from transverse tests). This compares well with the actual values at R = 0.1, which are 155 MPA in $c_f = 0.52$, 1/8 in. hole, 189 MPA for $c_f = 0.55$, 1/8 in. hole, and 155 MPA for $c_f = 0.55$, 3/8 in. hole; all at R = 0.1.

Of course, one should note that the maximum cyclic fiber stress is very high at the endurance limit. When the values of S^e are taken from Table III (172, 186, and 172 MPA at R = 0.1) and compared with the results of Figure 32, one finds that the maximum fiber stress is equal to about 1200 MPA, which is close to static strength of the fiber at 1380 MPa. The fiber stress is about twice as high in the specimens with holes,

as in the SL specimens at endurance limit. This, of course, is not an unusual occurrence in composite materials, and can be inferred from the work of Waddoups et al. (1971) and Whitney and Nuismer (1974).

In conclusion, the specimens with holes failed outside stress ranges which coincide with the calculated shakedown ranges. Actual values depend rather strongly on actual loading conditions. Larger holes and large negative values of R are obviously detrimental. Figure 33 summarizes the results. Theoretical prediction of failure stresses is difficult, if not impossible. Design information should be sought from experimental data.

To emphasize this point, Figures 34 and 35 show the stress ratios S_n/S_o, and S_n^e/S_o^e, from Table II. Both the hole size and the magnitude of the cyclic stress ratio R affect the measured values of S_n/S_o and S_n^e/S_o^e. The hole diameter appears to have a more significant effect on the reduction of endurance limits than on residual static strength. The stress ratio R has a small influence. However, note the comparatively large reduction of S_n^e/S_o^e at R = -5. No such effect on S_n/S_o is seen.

It is probably obvious that these results cannot be interpreted in terms of the models which are available for comparable reductions in static strength (Waddoups et al., 1971, Whitney and Nuisner, 1974). Therefore, the experimental points in Figures 34 and 35 are connected by straight lines for the sake of clarity of presentation. Additional tests with different hole sizes would be needed for construction of more accurate plots.

A reason for delamination of the specimens with holes tested in tension-compression can be found in the results of the numerical calcu-lations. When the compression stress is applied, it causes a transverse normal tensile strain, as well as a shear strain, at the lateral tangent

to the hole boundary. We recall from Figures 19, 20, 24, 25 that this tangent line is also the line of delamination. When these two strains are applied in a cyclic fashion, they apparently give rise to a delamination type shear crack.

A similar phenomenon is not observed in tension-tension fatigue of specimens with holes because the normal strain across the tangent is compressive. A quantitative evaluation of these strains at test conditions shown in Table IV may be of interest in a future investigation.

Reasons for the observed delamination of the SL specimens are unclear at this time.

7. CONCLUSIONS

Tension and compression, static and fatigue tests on notched and un-notched FP-Aℓ specimens suggest the following:

(i)   Fatigue endurance limits of FP-Aℓ specimens, with or without holes, are substantially lower than static strengths of these specimens. Reduction magnitudes depend on the applied cyclic stress ratio R. Tension endurance limits are in the range of 0.71 ÷ 0.84 of the residual tensile strength at R = 0.1, but this range is 0.53 ÷ 0.60 at R = -1, and 0.20 ÷ 0.31 at R = -5. Compression endurance limits are in the range of 0.14 ÷ 0.18 of static compressive strength at R = -1; at R = -5 this range is 0.21. (See Table II). Delamination is the principal damage mode in cyclic tension/compression tests.

(ii)   The unidirectional FP-Aℓ material is susceptible to delamination cracking in the longitudinal direction under cyclic tension/compression loading. This may be prevented or reduced by adding off-axis fiber layers.

(iii)   The magnitudes of both static strength and fatigue endurance limits are affected by the diameter of the drilled hole, and by the magnitude of R, c.f., Figures 34 and 35.

(iv)   Interpretation of the experimental results in terms of theoretical models appears possible only in a limited way. Specifically, it was found that the notched specimens do not fail when tested inside their shakedown range, Figure 3. This seems to suggest that failure in these specimens is related to cyclic plastic straining in the matrix, which occurs when the specimens are tested at

stress amplitudes which exceed the shakedown range of the specimen. However, this interpretation cannot be applied to unnotched SL specimens which fail within their shakedown range. Failure of these specimens appears to be caused by propagation of flaws which have been found in the as-fabricated material.

(v)   Endurance limits for FP-Aℓ specimens with different hole sizes, tested at different R ratios, can be determined only on the basis of experimental results. Reliable predictions cannot be made at this time.

ACKNOWLEDGEMENT

REFERENCES

Bahei-El-Din, Y.A., Dvorak, G.J. and Utku, S., (1981), Finite Element Analysis of Elastic-Plastic Fibrous Composite Structures, Computers and Structures, Vol. 13, p. 321.

Dvorak, G.J. and Wung, C.J., (1984), Thermoplasticity of Unidirectional Metal Matrix Composites, in Mechanics of Material Behavior, ed. by G.J. Dvorak and R.T. Shield, Elseiver, p. 87

Dvorak, G.J. and Johnson, W.S., (1980), Fatigue of Metal Matrix Composites, Intl. Jnl. of Fracture, v. 16, no. 6, p. 582.

Dvorak, G.J. and Rao, M.S.M., (1976), Thermal Stresses in Heat-Treated Fibrous Composites, Jnl. Applied Mechanics, Vol. 98, p. 619.

Dvorak, G.J. and Tarn, J.Q., (1975a), Fatigue and Shakedown in Metal Matrix Composites, ASTM-STP 569, p. 145.

Oplinger, D.W., Gandhi, K. and Parker, B., (1982), Studies of Tension Test Specimens for Composite Materials. Army Materials and Mechanics Research Center, AMMRC TR 82-27.

Tarn, J.Q., Dvorak, G.J. and Rao, M.S.M., (1975b), Shakedown of Unidirectional Composites, Intl. Jnl. Solids and Structures, v. 11, no. 6, p. 751.

Teply, J., (1984), Ph.D. Dissertation, University of Utah.

Tsangarakis, N., Slepetz, J.M. and Nunes, J., (1983), Fatigue Behavior of Alumina-Fiber Reinforced Aluminum Composites, Army Materials and Mechanics Research Center, AMMRC TR 83-52.

Waddoups, M.E., Eisenmann, J.R. and Kamiski, B.E., (1971), Macroscopic Fracture Mechanics of Advanced Composite Materials, J. Comp. Materials, p. 446.

Whitney, J.M. and Nuisner, R.J., (1974), Stress Fracture Criteria for Laminated Composites Containing Stress Concentrations, J. Comp. Materials, vol. 8, p. 253.

LIST OF TABLES

TABLE II Summary of Fatigue Test Results for FP-Aℓ

FIBER VOLUME c_f	SPECIMEN TYPE	R	ENDURANCE LIMIT S^e (Tension) MPa	ENDURANCE RANGE Δe MPa	$\frac{S^e_n}{S^e_o}$ R=constant	$\frac{\Delta e_n}{\Delta e_o}$ R=constant	RESIDUAL TENSION STRENGTH S MPa	$\frac{S_n}{S_o}$ R=constant	RESIDUAL* COMPRESSION STRENGTH S MPa	$\frac{S^e}{S}$ Tension	$\frac{S^e}{S}$ Compression
	transverse	0.1	83	75	1.0	1.0	167÷175	1.0		0.50	
	SL	0.1	407	366	1.0	1.0	541÷629	1.0		0.75	
0.52	1/8 in. hole	0.1	172	155	0.42	0.42	256	0.47		0.67	
	SL	0.1	455	409	1.0	1.0	600	1.0		0.76	
		-1.0	331	662	1.0	1.0	567	1.0	-1,813	0.58	0.18
		-5.0	172	1,032	1.0	1.0	546÷731	1.0		0.31	
	1/8 in. hole	0.1	210	189	0.46	0.46	248÷263	0.41	-1,310÷-1,405**	0.84	
0.55		-1.0	186	372	0.56	0.67	310	0.55		0.60	(0.14)
		-5.0	55	330	0.32	0.32	264÷354	0.48	-1,311	0.20	0.21
	3/8 in. hole	0.1	172	155	0.38	0.38	242	0.40		0.71	
		-1.0	124	248	0.38	0.45	233÷308	0.41		0.53	

* See discussion on p. 14 for proper interpretation of residual compression strength results.

** Static strength

( )Estimated value

TABLE III

Transversely Reinforced 1/2 in. Coupouns, $c_f = 0.52$, $R = 0.1$

No.	S_{max} psi	N cycles	Note	Residual Strength psi	MPa
1	19,040	6,760	Fatigue failure		
2	15,040	223,140	Fatigue failure		
3	13,550	13,620	Fatigue failure		
4	10,000 12,000	2×10^6 2×10^6	Runout Runout	24,200	167
5	13,550	872,820			
6	13,000	2×10^6	Runout	25,370	175
7	13,000	2×10^6	Runout	24,650	170
8	13,000	1,130,690	Fatigue failure		
9			Static tension	24,850	171

ENDURANCE LIMIT, $S_o^e = 12,000$ psi $= 83$ MPa

TABLE IV

SL Specimens, $c_f = 0.52$, $R = 0.1$

No.	S_{max} psi	N cycles	Note	Residual Strength psi	MPa
106-DK30-20	49,000	2×10^6	Runout	81,736	564
106-DK30-18	49,500	2×10^6	Runout		
	50,000	2×10^6	Runout	91,176	629
106-DK30-19	54,000	2×10^6	Runout	78,511	541
106-DK30-21	58,000	2×10^6	Runout		
	60,000	2×10^6	Runout		
	62,000	2×10^6	Runout		
	64,000	2×10^6	Runout		
	65,000	2×10^6	Runout		
	66,000	2×10^6	Runout		
	67,000	300,000	Fatigue failure		
106-DK30-36	62,000	1,609,000	Fatigue failure		
106-DK30-14	60,000	2×10^6	Runout		
	61,000	2×10^6	Runout		
	62,000	2×10^6	Runout		
	63,000	877,590	Fatigue failure		
106-DK30-15	60,000	61,140	Fatigue failure		

ENDURANCE LIMIT, $S_o^e = 59,000$ psi $= 407$ MPa

TABLE V

1/2 in. Coupons With 1/8 in. Holes, $c_f = 0.52$, $R = 0.1$

No.	S_{max} psi	N cycles	Note	Residual Strength psi	MPa
138-DJ5-20	13,132	1,450,000	Runout		
	17,000	2×10^6	Runout		
	19,500	2×10^6	Runout		
	21,500	2×10^6	Runout		
	23,500	2×10^6	Runout		
	27,500	383,300	Fatigue failure		
1n	17,000	2×10^6	Runout		
	19,500	2×10^6	Runout		
	21,500	2×10^6	Runout		
	23,500	2×10^6	Runout		
	25,500	1,099,000	Fatigue failure		
15	25,500	1,450,500	Fatigue failure		
138-DJ5-36	24,000	2×10^6	Runout		
	24,500	2×10^6	Runout		
	25,000	1,291,800	Runout		
	25,500	1,515,700	Runout	37,058	256
138-DJ5-37	24,000	2×10^6	Runout		
	24,500	2×10^6	Accidental failure		
138-DJ5-35	25,150	2×10^6	Runout		
	25,250	2×10^6	Runout		
	25,400	2×10^6	Runout		
	25,600	1,025,000	Fatigue failure		

ENDURANCE LIMIT, $S_n^e = 25,000$ psi $= 172$ MPa

TABLE VI

SL Specimens, $c_f = 0.55$, $R = 0.1$

No.	S_{max} psi	N cycles	Note	Residual Strength psi	MPa
83-FP-18	62,000	187,200	Fatigue failure		
83-FP-36	60,000	2×10^6	Runout		
	62,000	2×10^6	Runout		
	64,000	2×10^6	Runout		
	66,000	2×10^6	Runout		
	68,000	166,400	Fatigue failure		
83-FP-32	66,000	2×10^6	Runout		
	68,000	101,200	Fatigue failure		
83-FP-22			Static tension	98,831	681
83-FP-23	66,000	2×10^6	Runout		
	67,000	2×10^6	Runout		
	67,500	52,300	Fatigue failure		
83-FP-1	66,000	2×10^6	Runout		
	67,000	2×10^6	Runout		
	67,500	2×10^6	Runout		
	68,000	101,700	Fatigue failure		

ENDURANCE LIMIT, $S_o^e = 66,000$ psi = 455 MPa

TABLE VII

SL Specimens, $c_f = 0.55$, R = -1

No.	S_{max} psi	N cycles	Note	Residual Strength psi	MPa
83-FP-13	50,000	1,902,000	Fatigue failure		
83-FP-10	52,000	2×10^6	Runout		
	54,000	1,624,300	Fatigue failure		
83-FP-21	48,000	1×10^6	Runout	82,235	567
83-FP-25	48,000	2×10^6	Runout		
	50,000	2×10^6	Runout		
	52,000	2×10^6	Static compression	-262,945	-1,813
83-FP-29	48,000	2×10^6	Runout		
	50,000	606,500	Fatigue failure		
83-FP-38	48,000	2×10^6	Runout		
	50,000	2×10^6	Runout	83,196	574
83-FP-41	50,000	2×10^6	Runout		
			Static compression	-270,148	-1,863

ENDURANCE LIMIT, S_o^e = 48,000 psi = 331 MPa
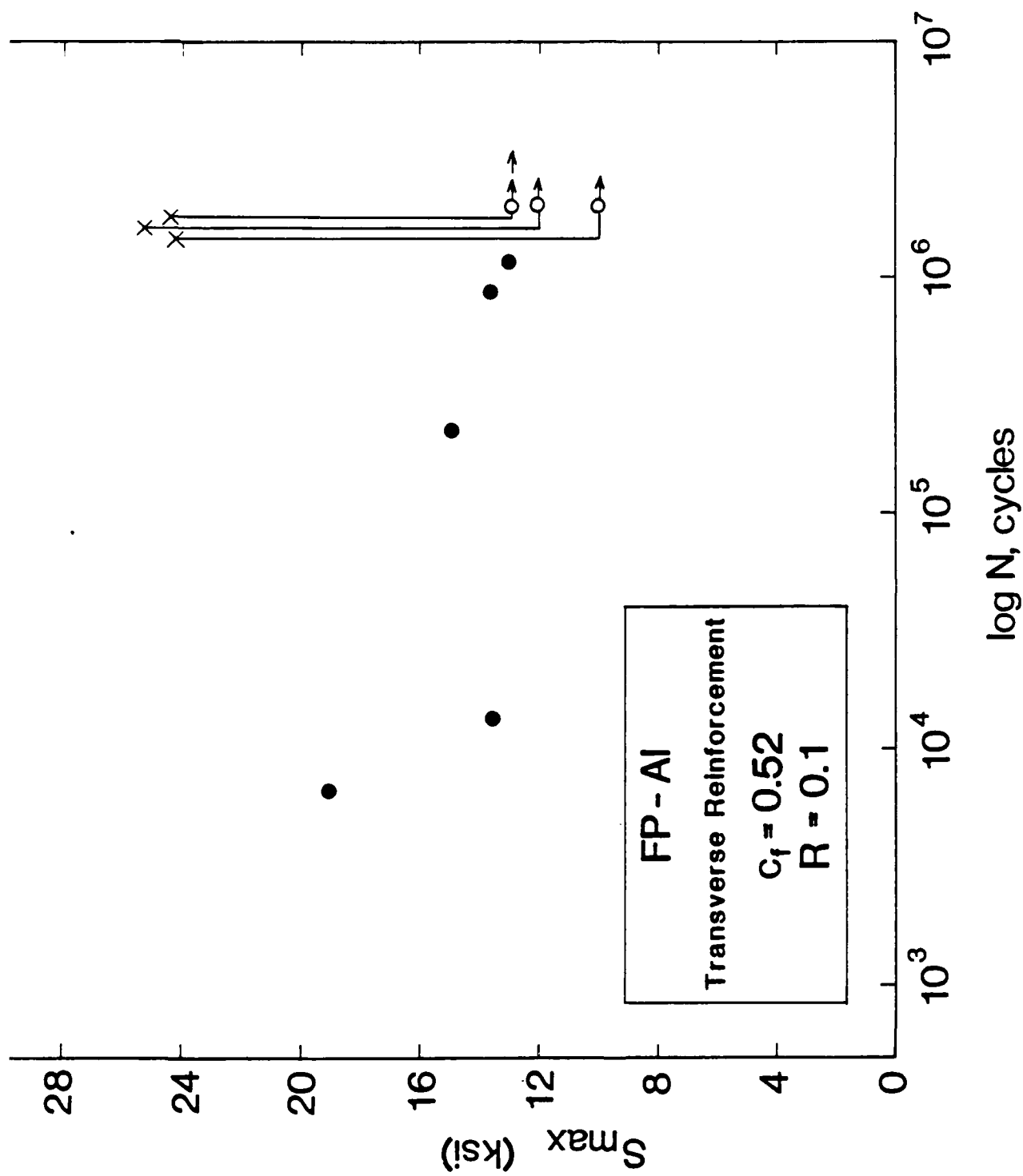
Figure 3.   Fatigue test results for transversely reinforced 0.5 in. wide coupons
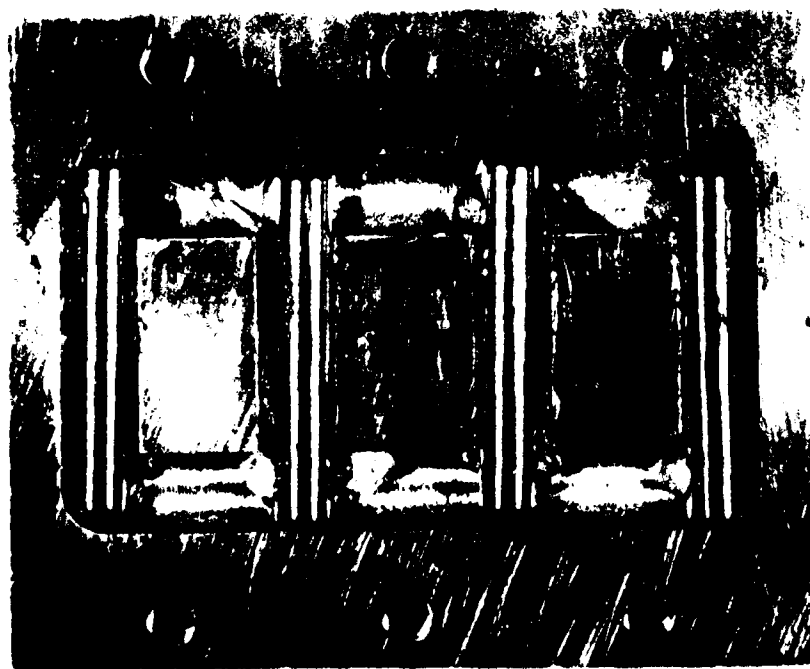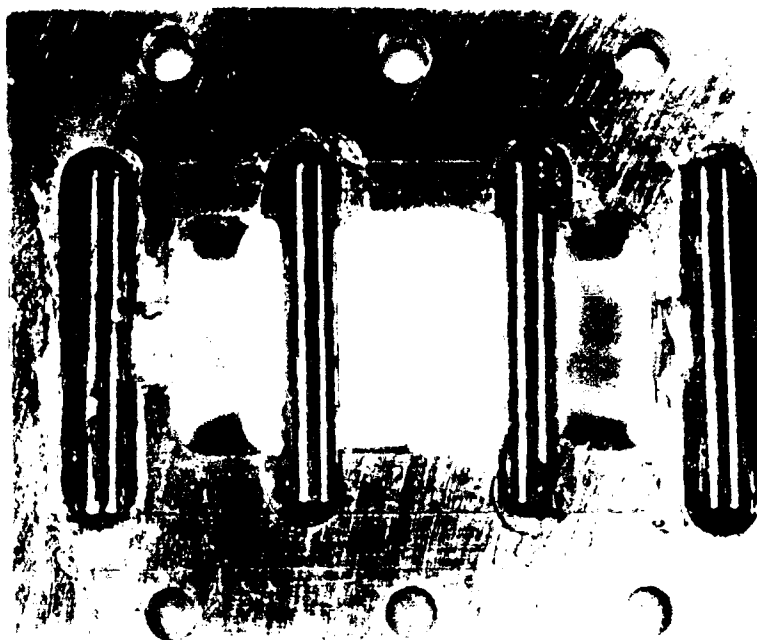
2d. Antibuckling plattens
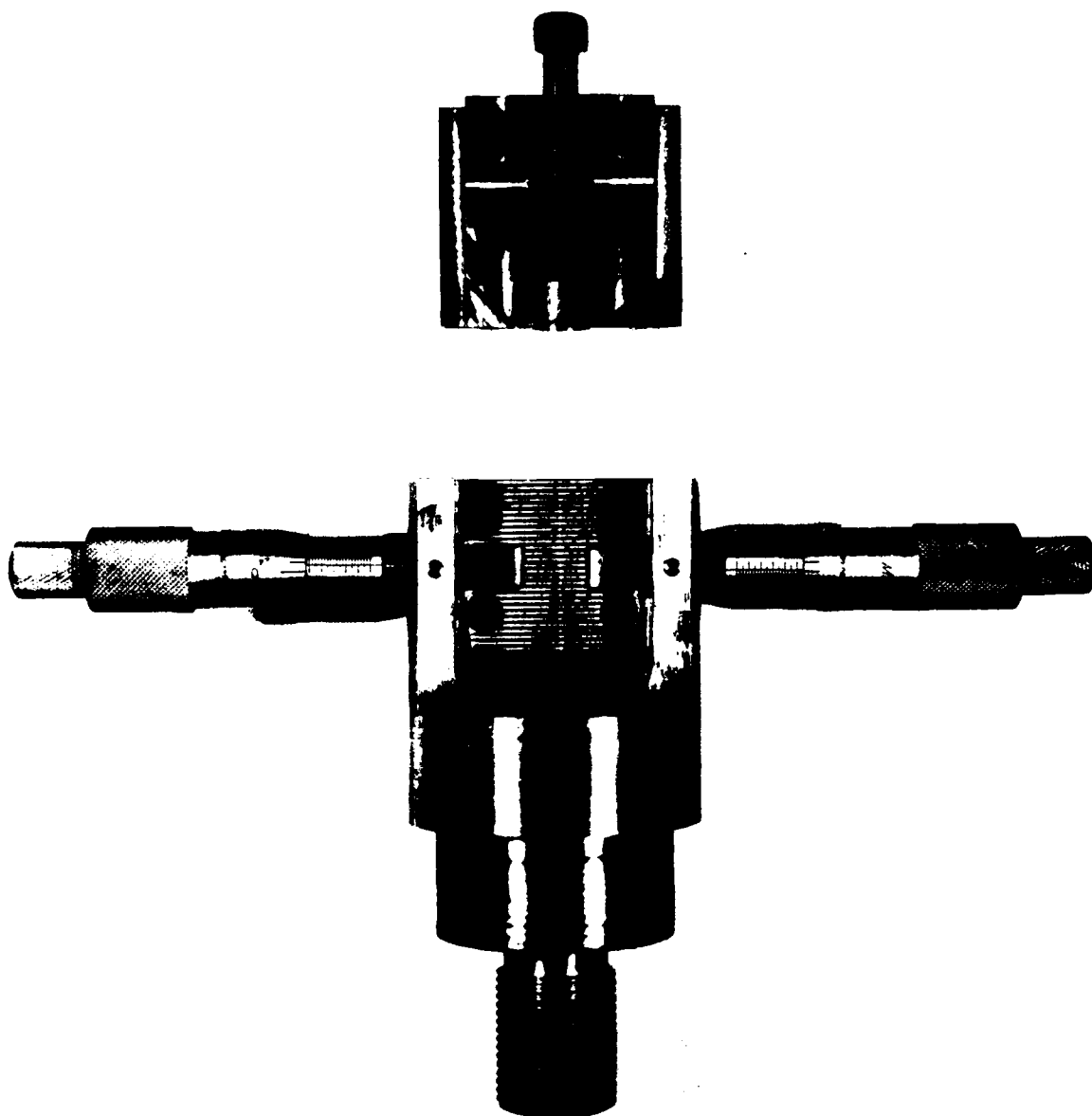
2c. Disassembled parts of the grip with tapered lateral
     micrometers for alignment of specimens
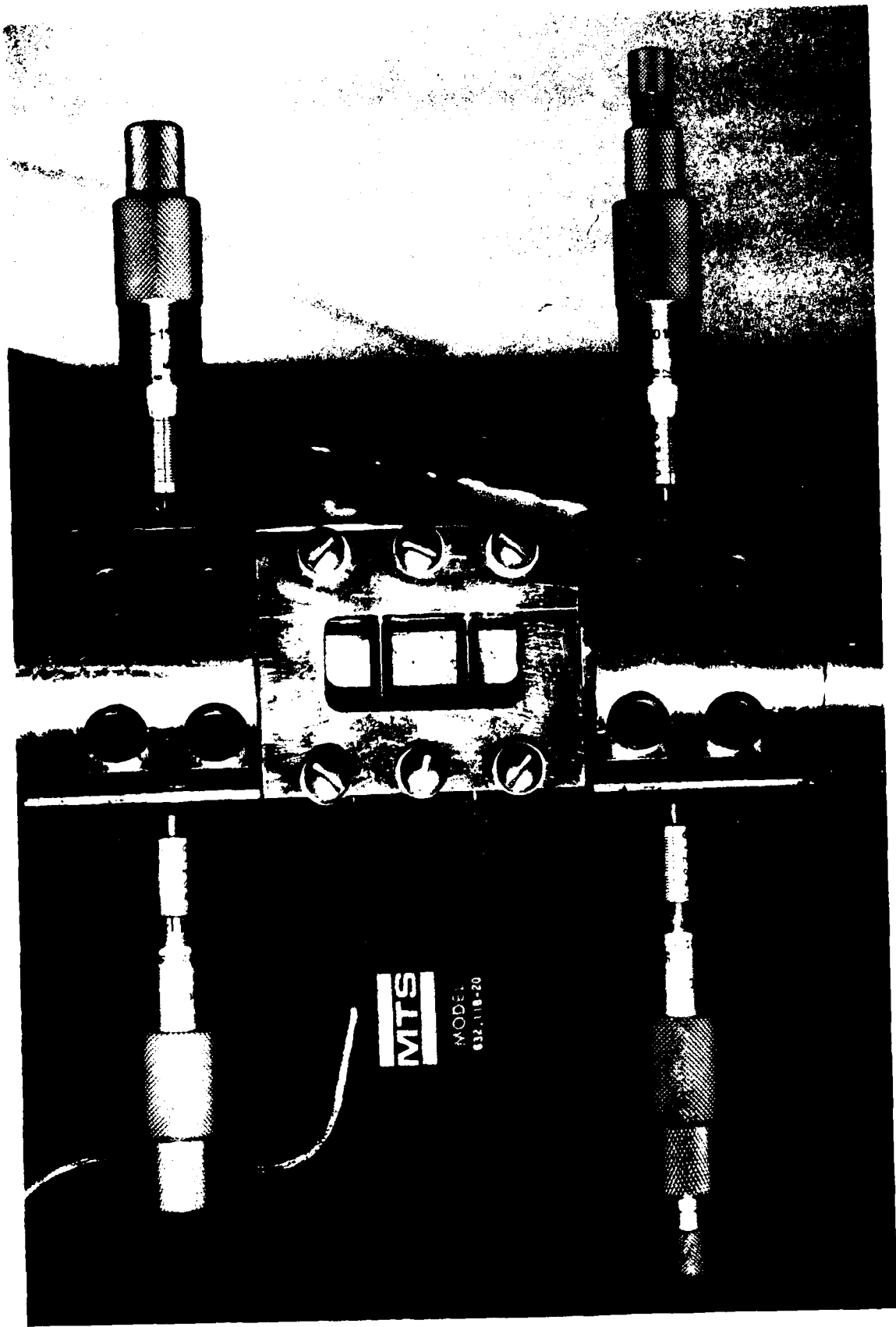
2b. Close-up view of assembled tension-compression grips
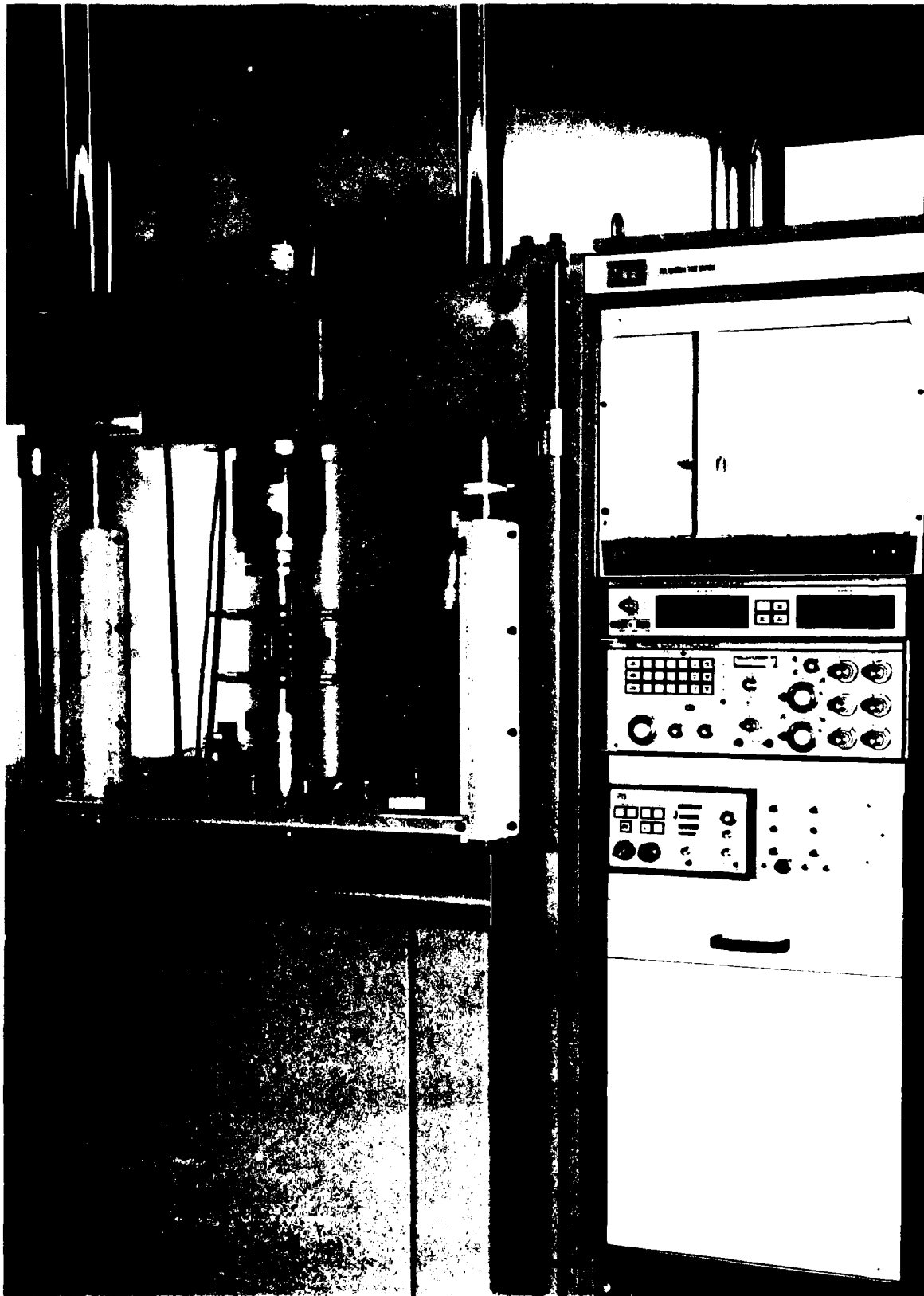
Figure 2a. Tension-compression grips in the 55 kip MTS machine

Figure 1.   Dimensions of specimens

LIST OF FIGURES

TABLE XIII

1 1/2 in. Coupons With 3/8 in. Holes, $c_f = 0.55$, $R = -1$

No.	S_{max} psi	N cycles	Note	Residual Strength psi	MPa
B-1-I	26,000	1,000,000	Delamination		
	26,000	1,000,000	Runout	49,200	270
B-2-I	22,000	1,500,000	Delamination		
	22,000	500,000	Runout	44,740	308
B-3-I	15,000	2×10^6	Runout		
	18,000	2×10^6	Runout		
	21,000	2×10^6	Delamination	34,421	237
B-1-II	18,000	2×10^6	Runout		
	20,000	1,500,000	Delamination	35,056	242
B-2-II	16,000	2×10^6	Runout		
	18,000	2×10^6	Runout		
	20,000	1,200,000	Delamination	40,353	278
B-3-II	17,000	2×10^6	Runout		
	19,000	2×10^6	Delamination	39,039	269
B-1-III	17,000	2×10^6	Runout		
	19,000	2×10^6	Runout		
	20,000	2×10^6	Runout		
	22,000	2×10^6	Delamination	33,859	233
B-2-III	19,000	2×10^6	Runout		
	22,000	2×10^6	Delamination	39,355	271
B-3-III	21,000	2×10^6	Runout		
	22,000	2×10^6	Delamination	34,870	240

ENDURANCE LIMIT, $S_n^e = 18,000$ psi $= 124$ MPa

TABLE XII

1 1/2 in. Coupons With 3/8 in. Holes, $c_f = 0.55$, R = 0.1

No.	S_{max} psi	N cycles	Note	Residual Strength psi	MPa
B-14-IV	15,000	2×10^6	Runout		
	18,000	2×10^6	Runout		
	21,000	2×10^6	Runout		
	24,000	2×10^6	Runout		
	26,000	1,834,000	Fatigue failure		
B-27-II	23,000	2×10^6	Runout		
	24,000	2×10^6	Runout		
	25,000	2×10^6	Runout		
	26,000	2×10^6	Runout	35,123	242
B-15-IV	24,000	2×10^6	Runout		
	25,000	2×10^6	Runout		
	26,000	2×10^6	Runout		
	27,000	2×10^6	Runout		
	28,000	2×10^6	Runout		
	29,000	500,000	Runout		
	30,000	1,500,000	Runout		
	32,000	233,800	Fatigue failure		
B-13-IV	24,000	2×10^6	Runout		
	26,000	2×10^6	Runout		
	28,000	2×10^6	Runout		
	30,000	2×10^6	Runout		
	32,000	2×10^6	Runout		
	34,000	62,300	Fatigue failure		
B-13-III	28,000	2×10^6	Runout		
	30,000	2×10^6	Runout		
	32,000	31,300	Fatigue failure		
B-15-III	28,000	2,800	Fatigue failure		

ENDURANCE LIMIT, S_n^e = 25,000 psi = 172 MPa

TABLE XI

1/2 in. Coupons With 1/8 in. Holes, $c_f = 0.55$, R = -5

No.	S_{max} psi	N cycles	Note	Residual Strength psi	MPa
83-FP-2	12,000	200,000	Delamination		
	12,000	1,800,000	Runout		
	15,000	2×10^6	Runout		
	18,000	1,321,500	Fatigue failure		
83-FP-26	15,000	7,500	Delamination		
	15,000	1,992,500	Runout		
	18,000	219,300	Fatigue failure		
83-FP-39	8,000	1,000,000	Runout		
	12,000	954,200	Delamination		
			Static compression	-200,113	-1,380
83-FP-33	10,000	435,000	Delamination		
	10,000	1,400,000	Runout	51,352	354
83-FP-35	6,000	2×10^6	Runout		
	8,000	2×10^6	Runout		
	10,000	1,214,200	Delamination	38,309	264
83-FP-6	6,000	2×10^6	Runout		
	8,000	2×10^6	Runout		
	10,000	2×10^6	Delamination		
			Static compression	-190,116	-1,311

ENDURANCE LIMIT, S_n^e = 8,000 psi = 55 MPa

TABLE X

1/2 in. Coupons With 1/8 in. Holes, $c_f = 0.55$, $R = -1$

No.	S_{max} psi	N cycles	Note	Residual Strength psi	MPa
83-FP-5	12,000	2×10^6	Runout		
	14,000	2×10^6	Runout		
	16,000	2×10^6	Runout		
	18,000	2×10^6	Runout		
	20,000	2×10^6	Runout		
	22,000	2×10^6	Runout		
	24,000	2×10^6	Runout		
	26,000	2×10^6	Runout		
	28,000	1,254,500	Fatigue failure		
83-FP-8	24,000	2×10^6	Runout		
	26,000	2×10^6	Runout		
	28,000	2×10^6	Runout		
	30,000	850,000	Fatigue failure		
83-FP-20	26,000	2×10^6	Runout		
	28,000	2×10^6	Runout		
	30,000	2×10^6	Runout		
	32,000	1,900,000	Fatigue failure		
83-FP-12	27,000	2×10^6	Runout		
	29,000	105,000	Fatigue failure		
83-FP-9	27,000	2×10^6	Runout		
	29,000	2×10^6	Runout		
	31,000	2×10^6	Runout		
	33,000	1,193,200	Runout	45,029	310
83-FP-37	28,000	500,000	Fatigue failure		

ENDURANCE LIMIT, $S_n^e = 27,000$ psi = 186 MPa

TABLE IX

1/2 in. Coupons With 1/8 in. Holes, $c_f = 0.55$, $R = 0.1$

No.	S_{max} psi	N cycles	Note	Residual Strength psi	MPa
83-FP-19	22,500	2×10^6	Runout		
	23,500	2×10^6	Runout		
	24,500	2×10^6	Runout		
	25,500	2×10^6	Runout		
	26,500	2×10^6	Runout		
	27,500	2×10^6	Runout		
	28,500	2×10^6	Runout		
	29,500	2×10^6	Runout		
	30,500	2×10^6	Runout		
	31,500	304,700	Fatigue failure		
83-FP-27	27,500	2×10^6	Runout		
	28,500	2×10^6	Runout		
	29,500	2×10^6	Runout		
	30,500	2×10^6	Runout		
	31,500	301,200	Fatigue failure		
83-FP-4	30,500	2×10^6	Runout	37,950	262
83-FP-3	29,500	1×10^6	Runout		
	30,500	2×10^6	Runout	36,367	251
83-FP-24	29,500	2×10^6	Runout		
	30,500	2×10^6	Runout	38,104	263
83-FP-14			Static compression	-203,732	-1,405
83-FP-17			Static compression	-194,218	-1,339
83-FP-40			Static tension	35,962	248
83-FP-6			Static compression	-189,927	-1,310

ENDURANCE LIMIT, $S_n^e = 30,500$ psi $= 210$ MPa

TABLE VIII

SL Specimens, $c_f = 0.55$, $R = -5$

No.	S_{max} psi	N cycles	Note	Residual Strength psi	MPa
83-FP-28	18,000	2×10^6	Runout		
	20,000	2×10^6	Runout		
	23,000	2×10^6	Runout		
	26,000	2×10^6	Runout		
	29,000	300	Fatigue failure		
83-FP-11	15,000	2×10^6	Runout		
	19,000	2×10^6	Runout		
	22,000	2×10^6	Runout		
	26,000	2×10^6	Runout		
	28,000	542,800	Fatigue failure		
83-FP-30	25,000	2×10^6	Runout		
	27,000	88,870	Fatigue failure		
83-FP-31	26,000	2×10^6	Runout	79,232	546
83-FP-7	25,000	2×10^6	Runout		
	26,000	2×10^6	Runout	101,020	697
83-FP-15	25,000	2×10^6	Runout		
	26,000	286,790	Fatigue failure		
83-FP-16	25,000	2×10^6	Runout		
	27,000	2×10^6	Runout	106,070	731

ENDURANCE LIMIT, $S_o^e = 25,000$ psi = 172 MPa
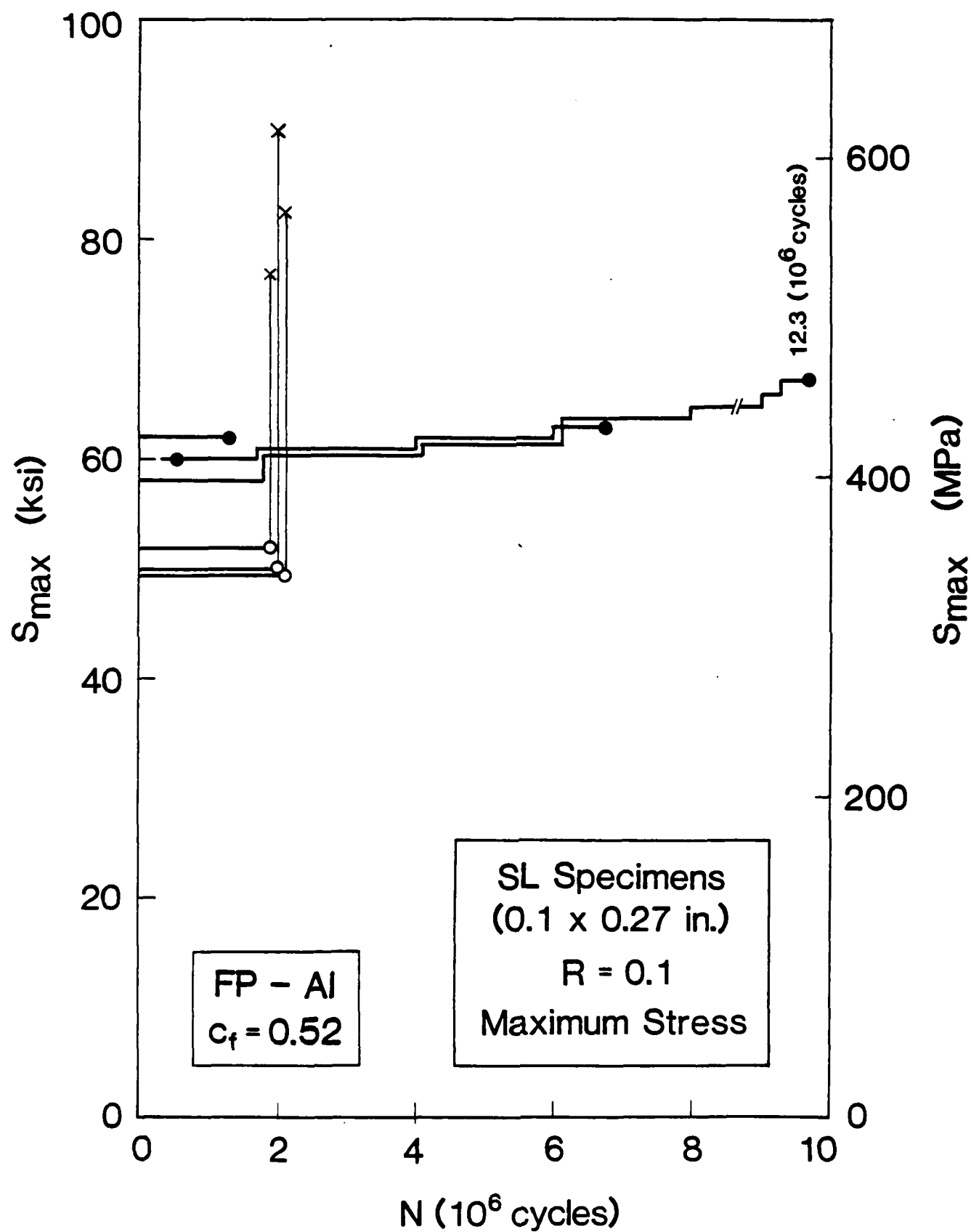
Figure 4.   Fatigue test results for longitudinally reinforced SL specimens
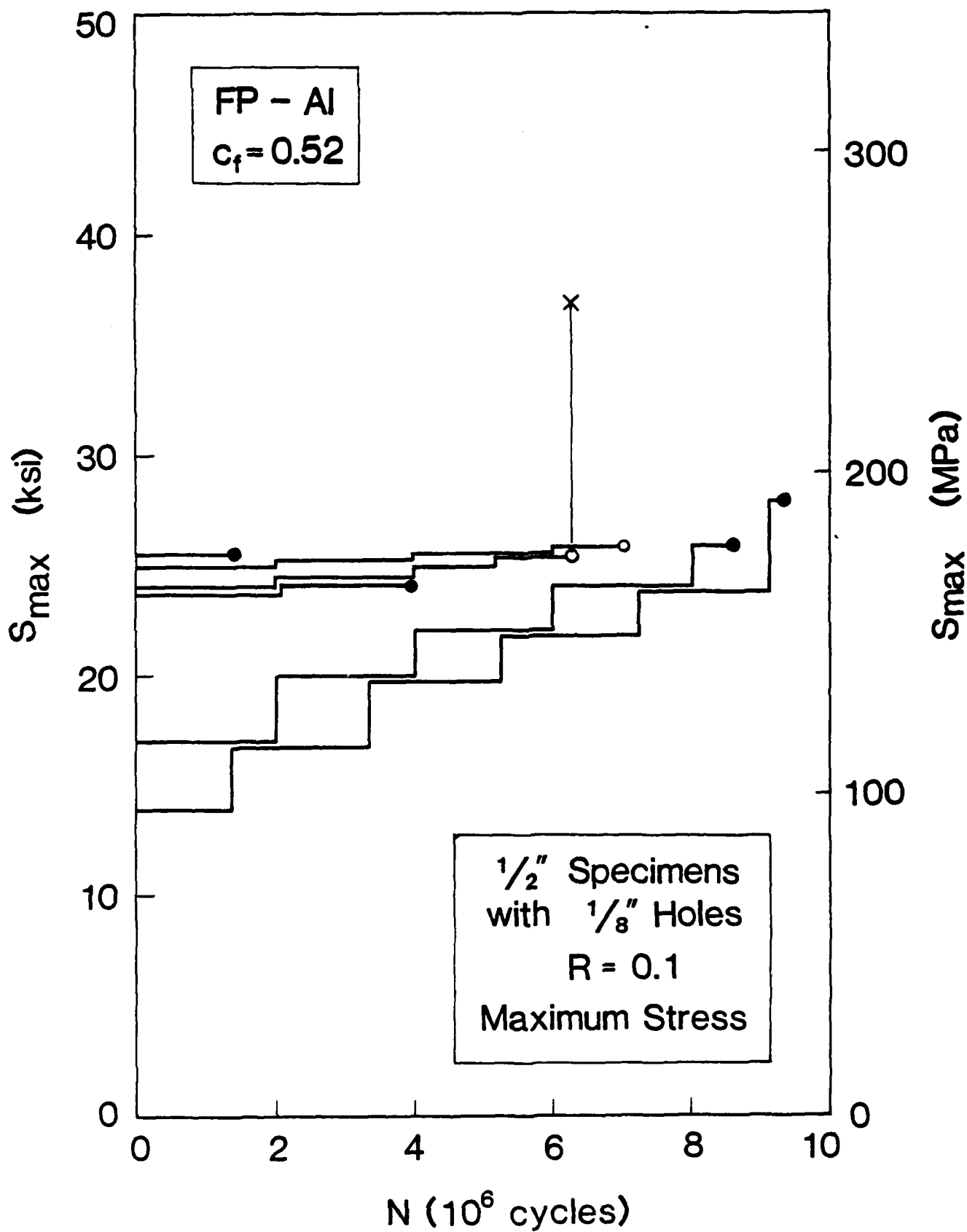
Figure 5. Fatigue test results for longitudinally reinforced coupons with a drilled hole
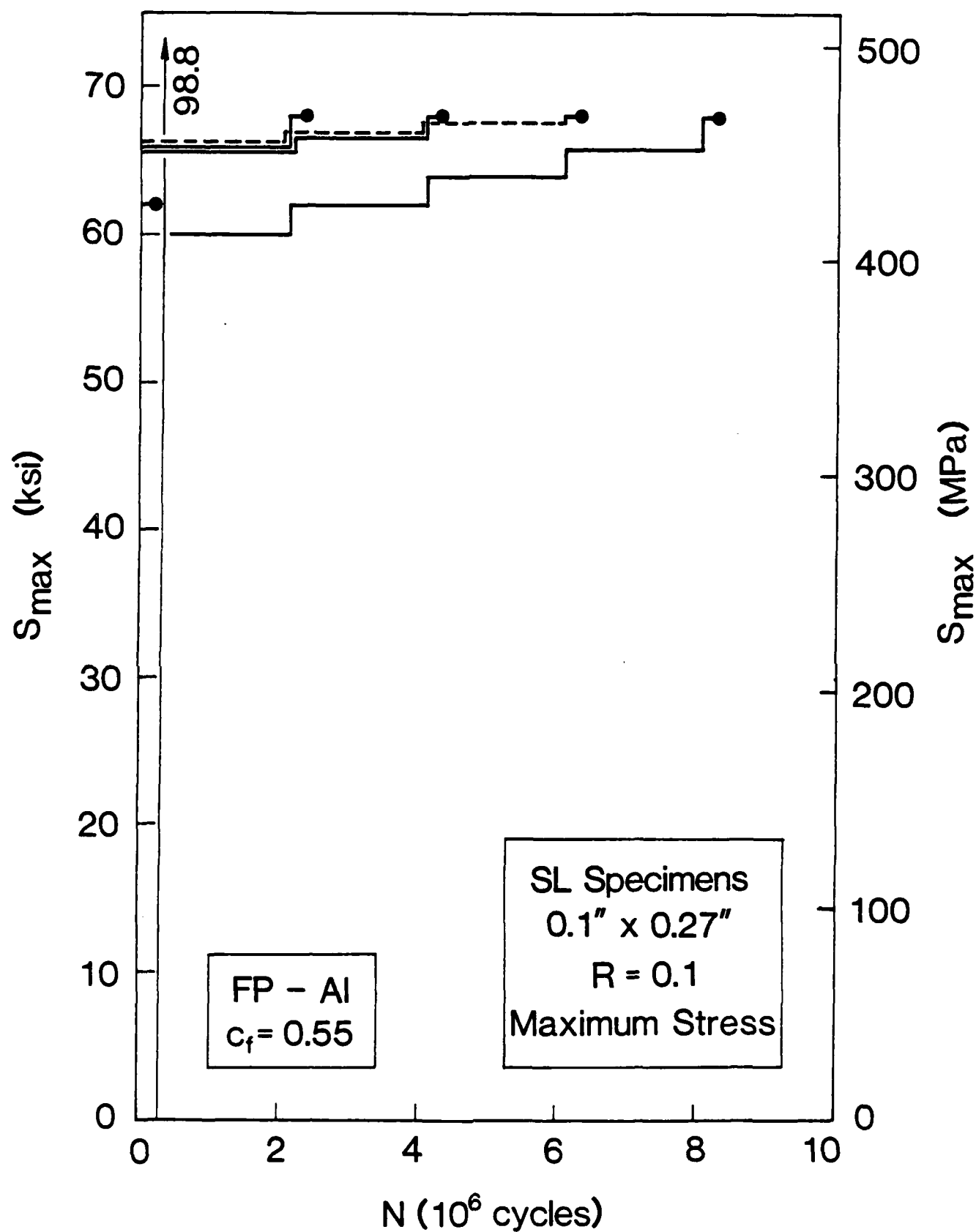
Figure 6.   Fatigue test results for SL samples, R = 0.1
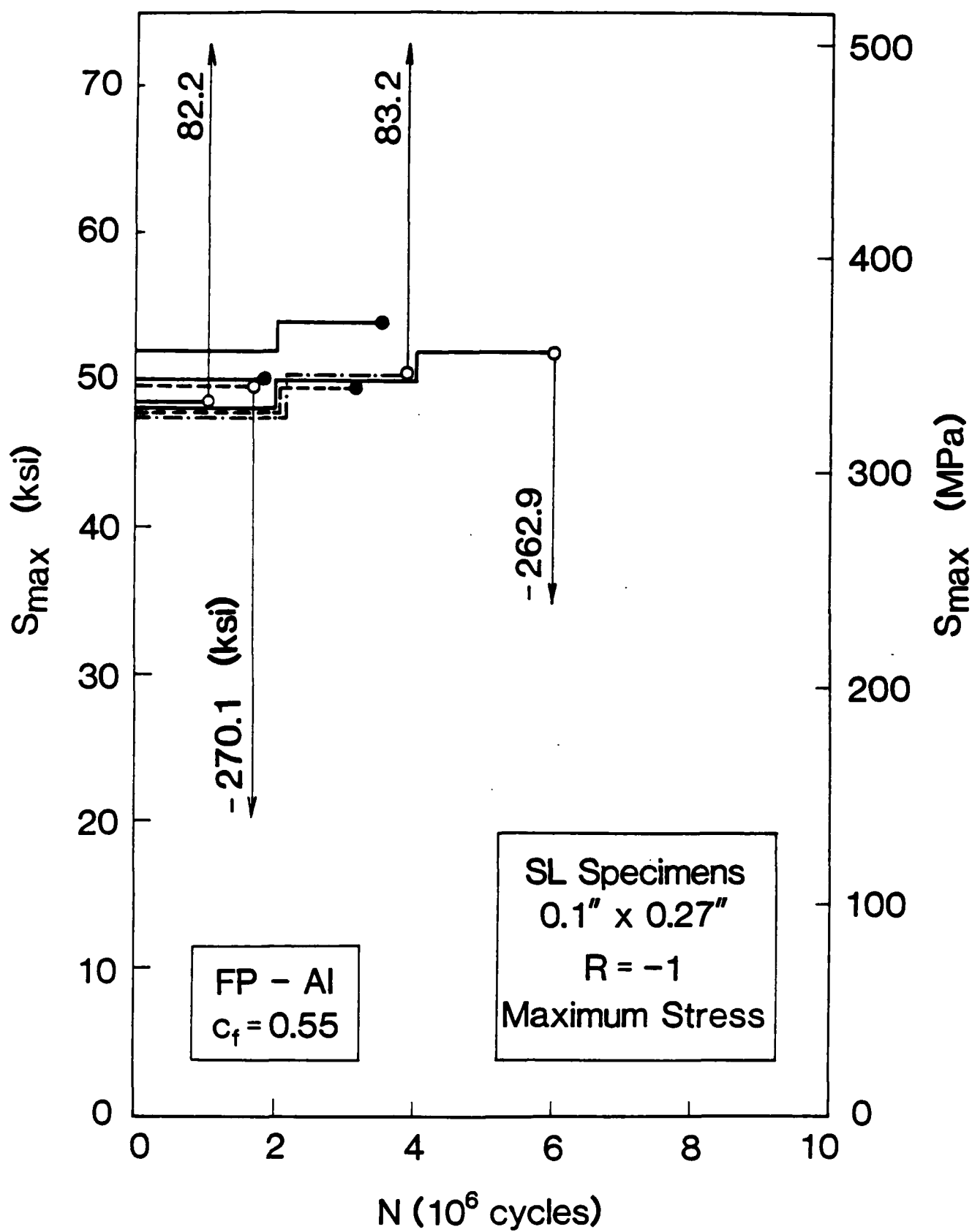
Figure 7.   Fatigue test results for SL samples, R = -1
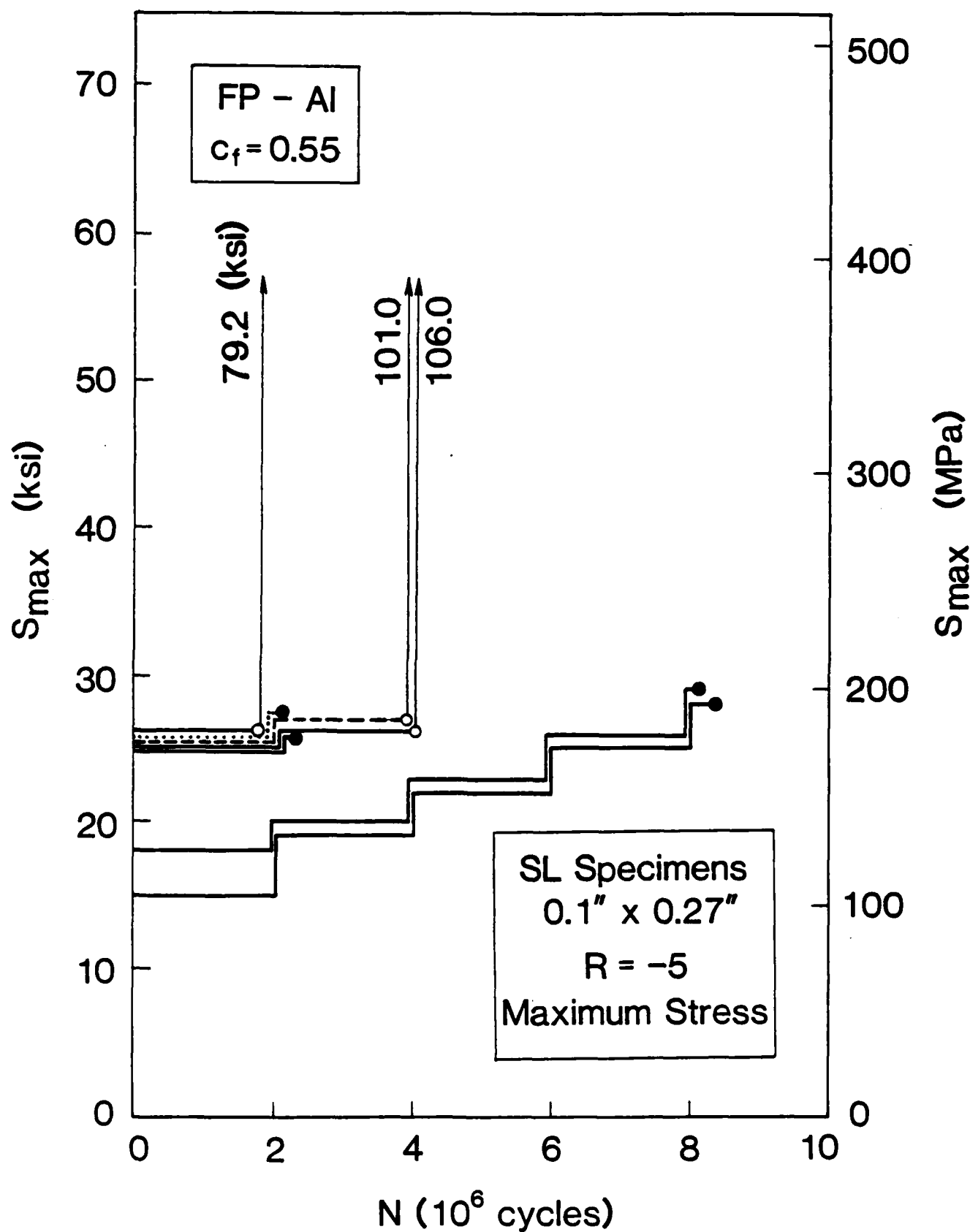
Figure 8.   Fatigue test results for SL samples, R = -5

83-FP-1
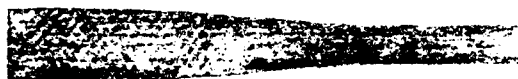
83-FP-18
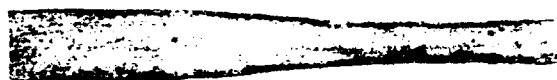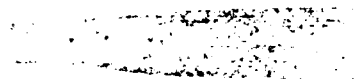
83-FP-22
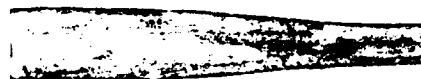
83-FP-23
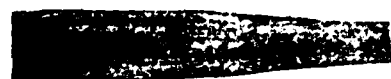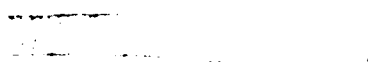
83-FP-32
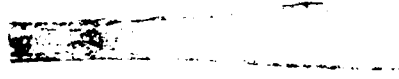
83-FP-36
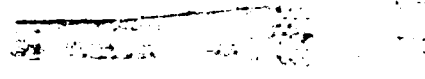
Figure 9.   Broken SL test specimens, R = 0.1

83-FP-10

83-FP-13
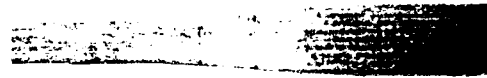
83-FP-21

83-FP-25

83-FP-29
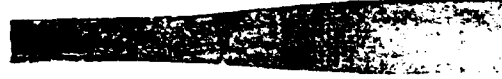
83-FP-38
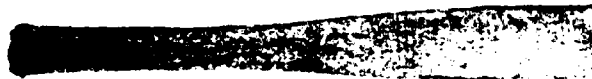
83-FP-41

Figure 10.   Broken SL test specimens, R = -1

83-FP-7

83-FP-11
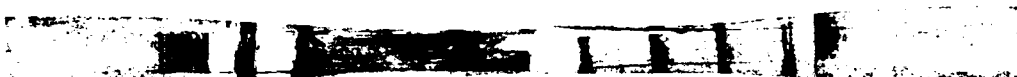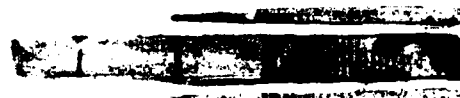
83-FP-15

83-FP-16

83-FP-28
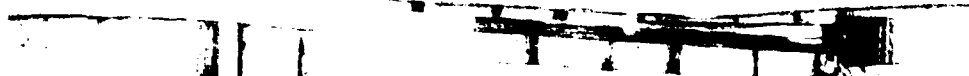
83-FP-30
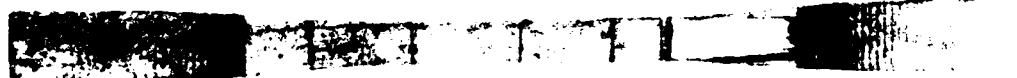
83-FP-31

Figure 11. Broken SL test specimens, R = -5
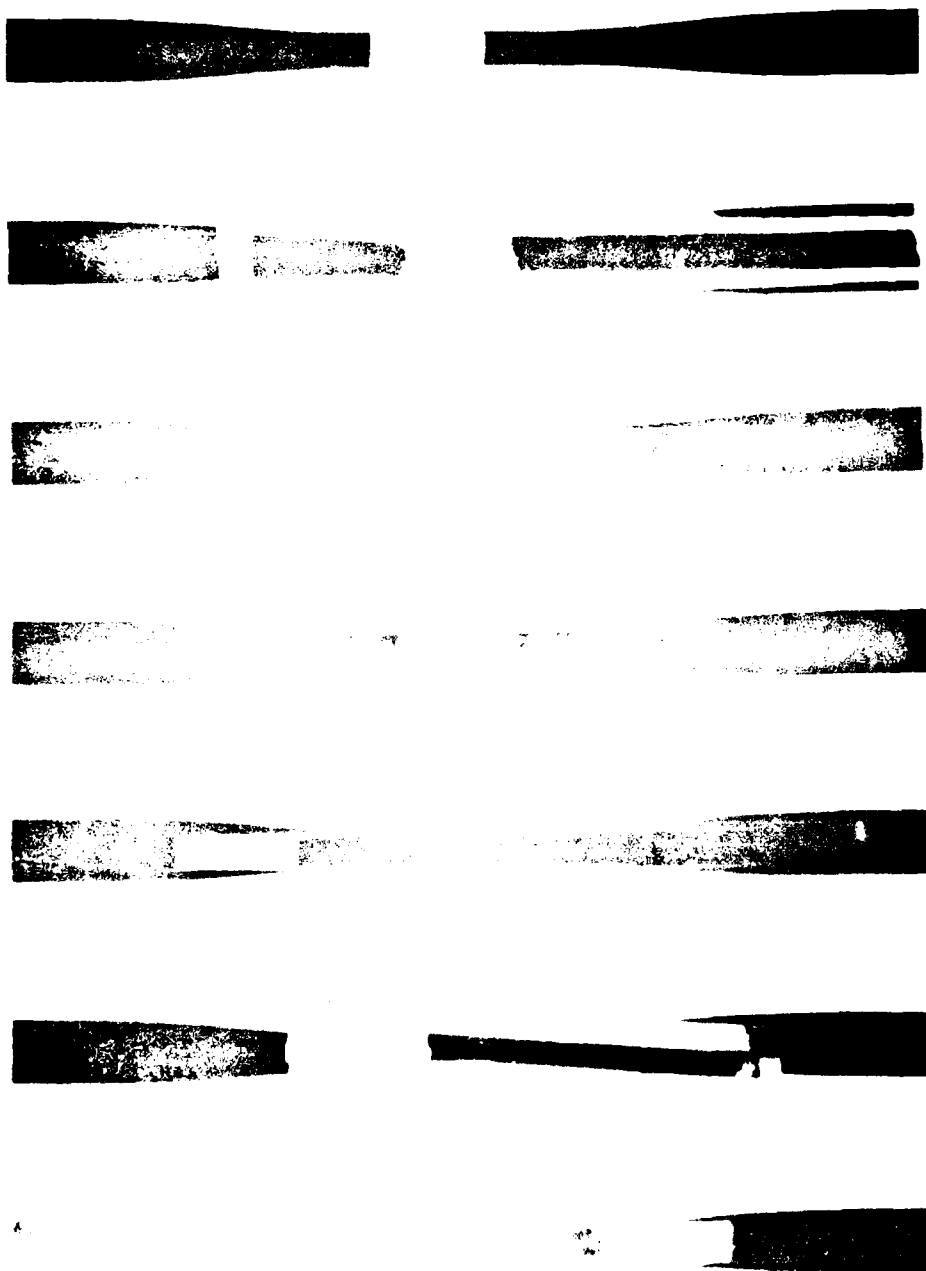
Figure 12. Radiograph of broken SL test specimens, R = -5
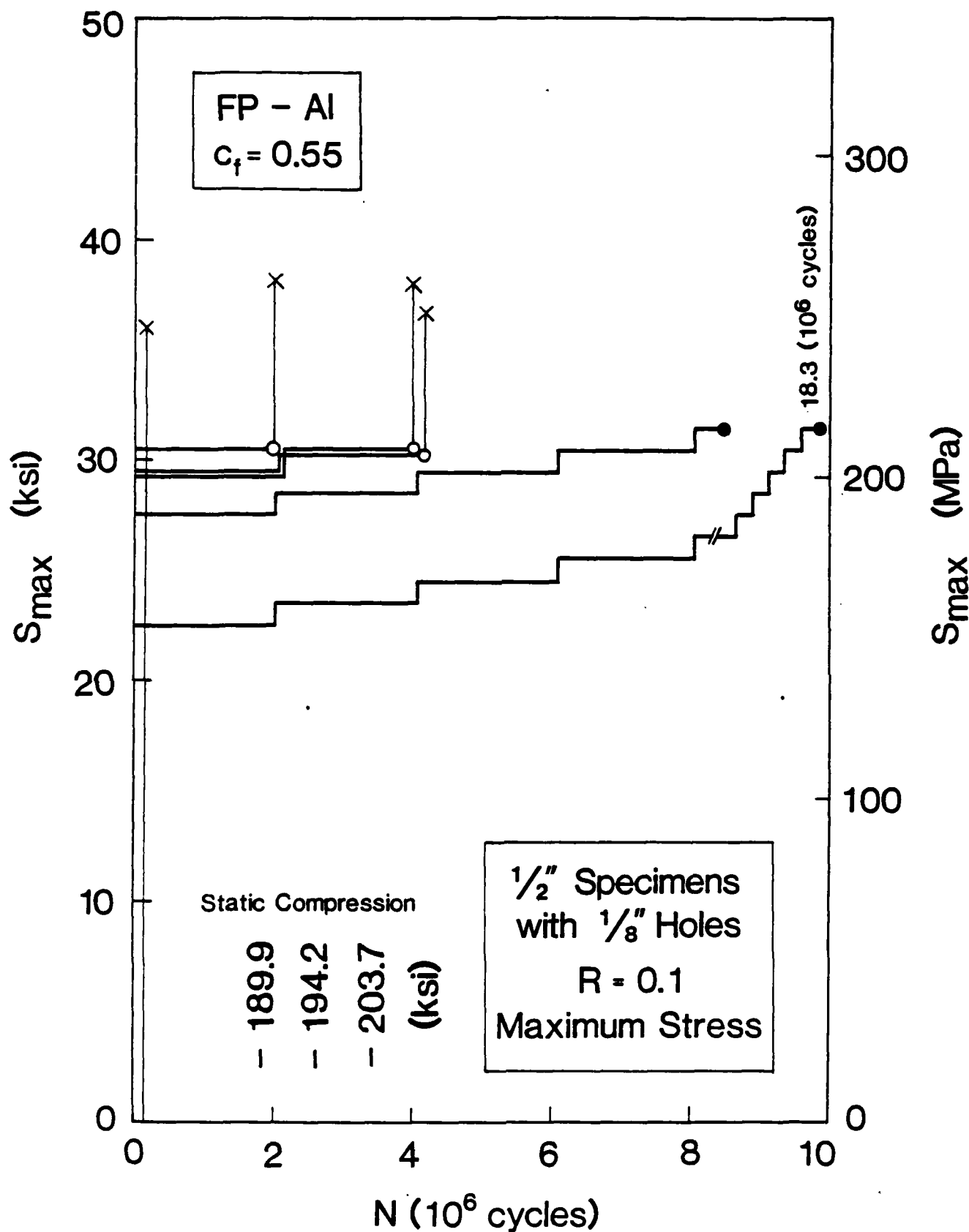
Figure 13.   Fatigue test results for 1/2 in. coupons with drilled holes,
R = 0.1
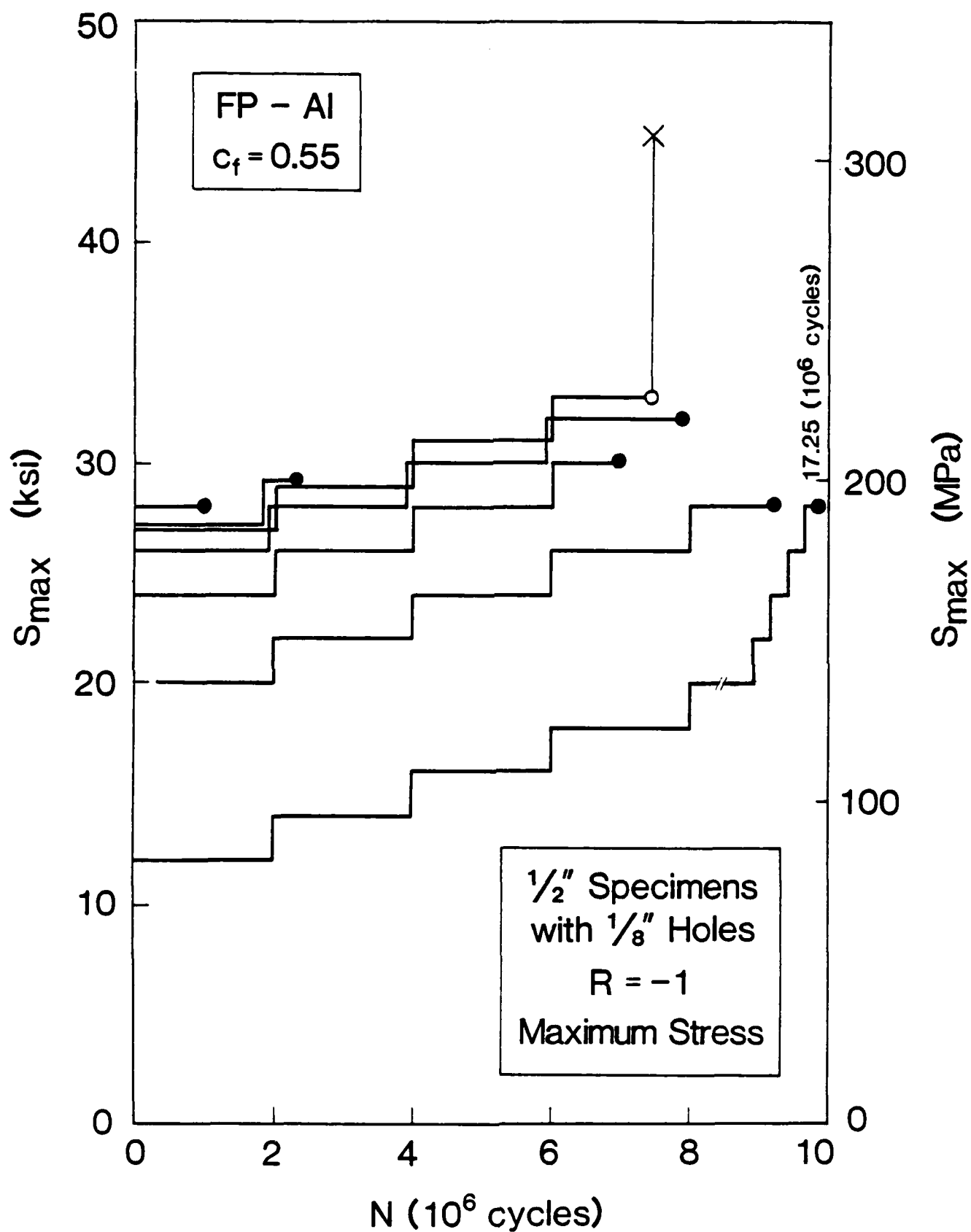
Figure 14.   Fatigue test results for 1/2 in. coupons with drilled holes,
             R = -1
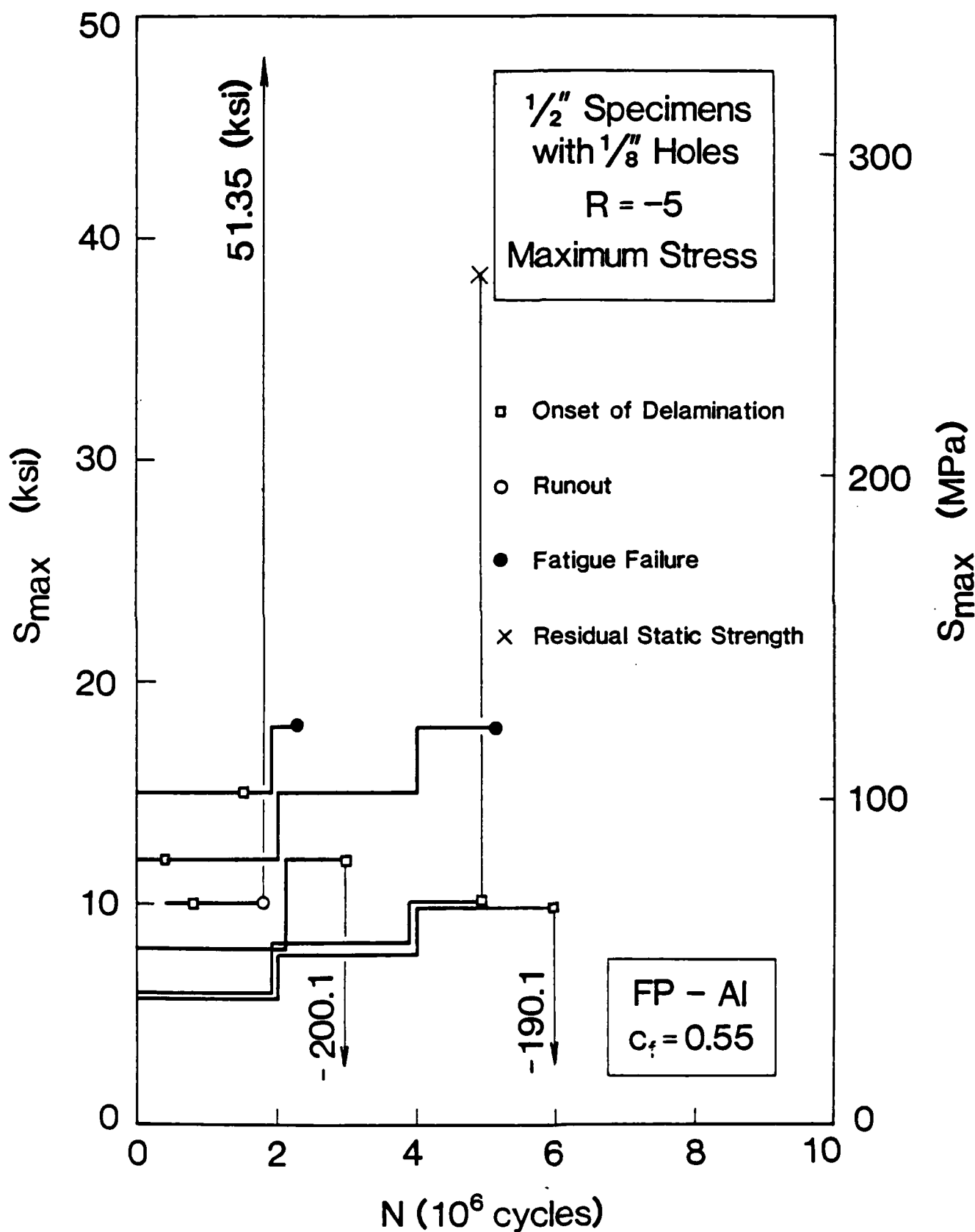
Figure 15.   Fatigue test results for 1/2 in. coupons with drilled holes, R = -5
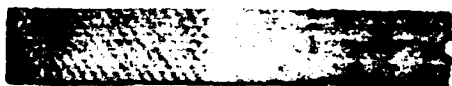
83-FP-3

83-FP-4
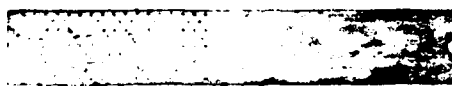
83-FP-24
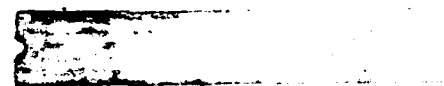
83-FP-27

Figure 16.   Broken test specimens with 1/8 in. hole, R = 0.1

83-FP-5

83-FP-8
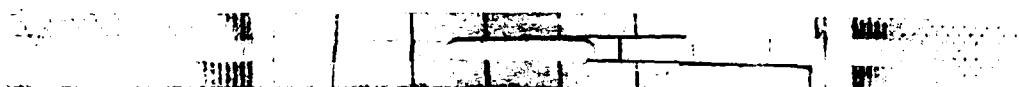
83-FP-9
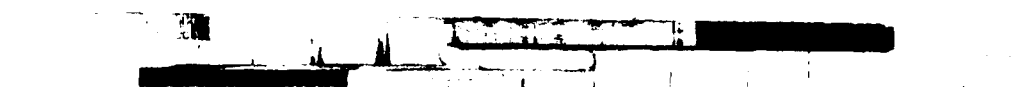
83-FP-12

83-FP-14

83-FP-17

83-FP-20

83-FP-37

83-FP-40

Figure 17.   Broken test specimens with 1/8 in. hole, R = -1 and static
             compression tests
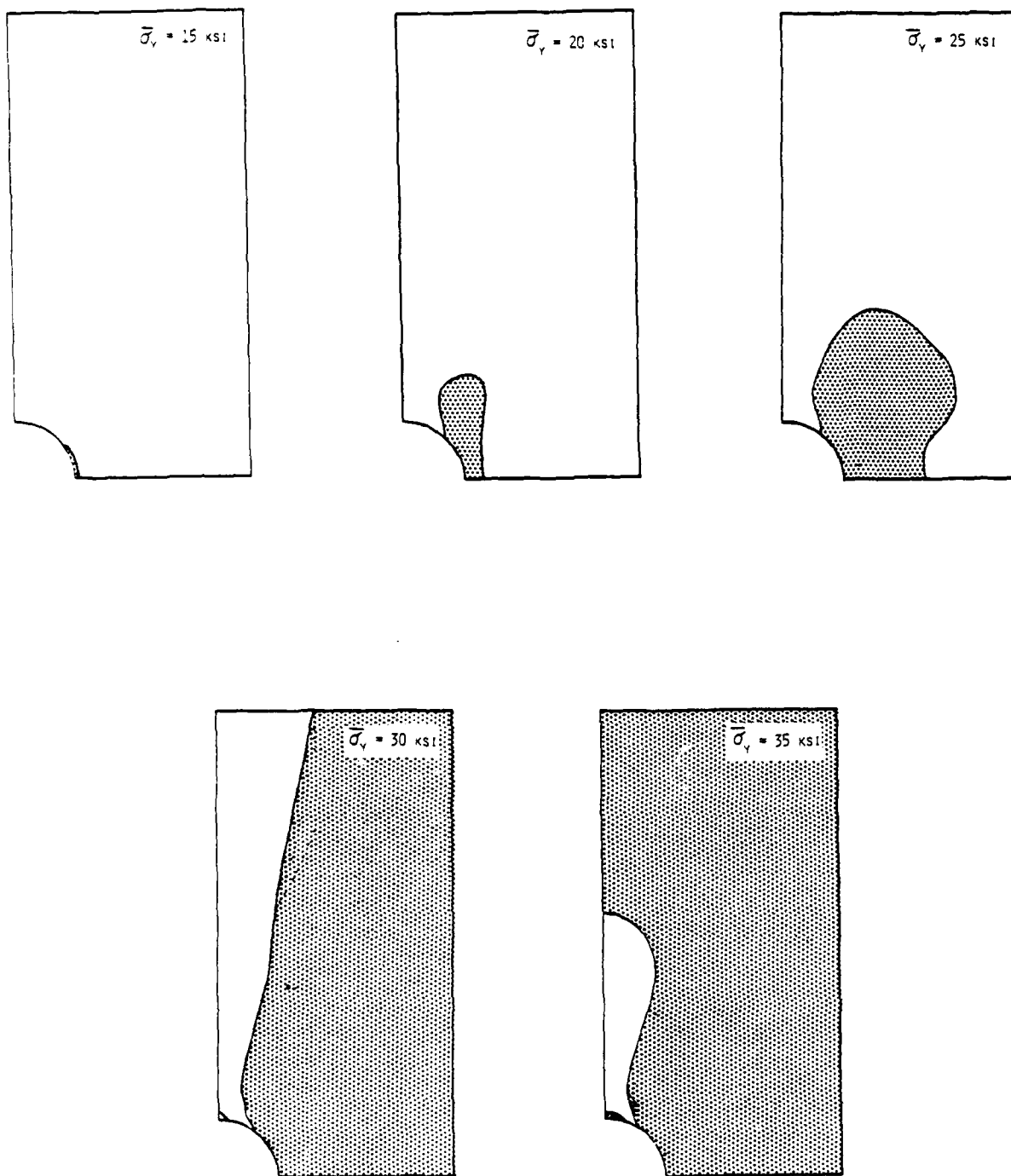
Figure 31. Development of plastic zones during loading of the specimen with a circular hole
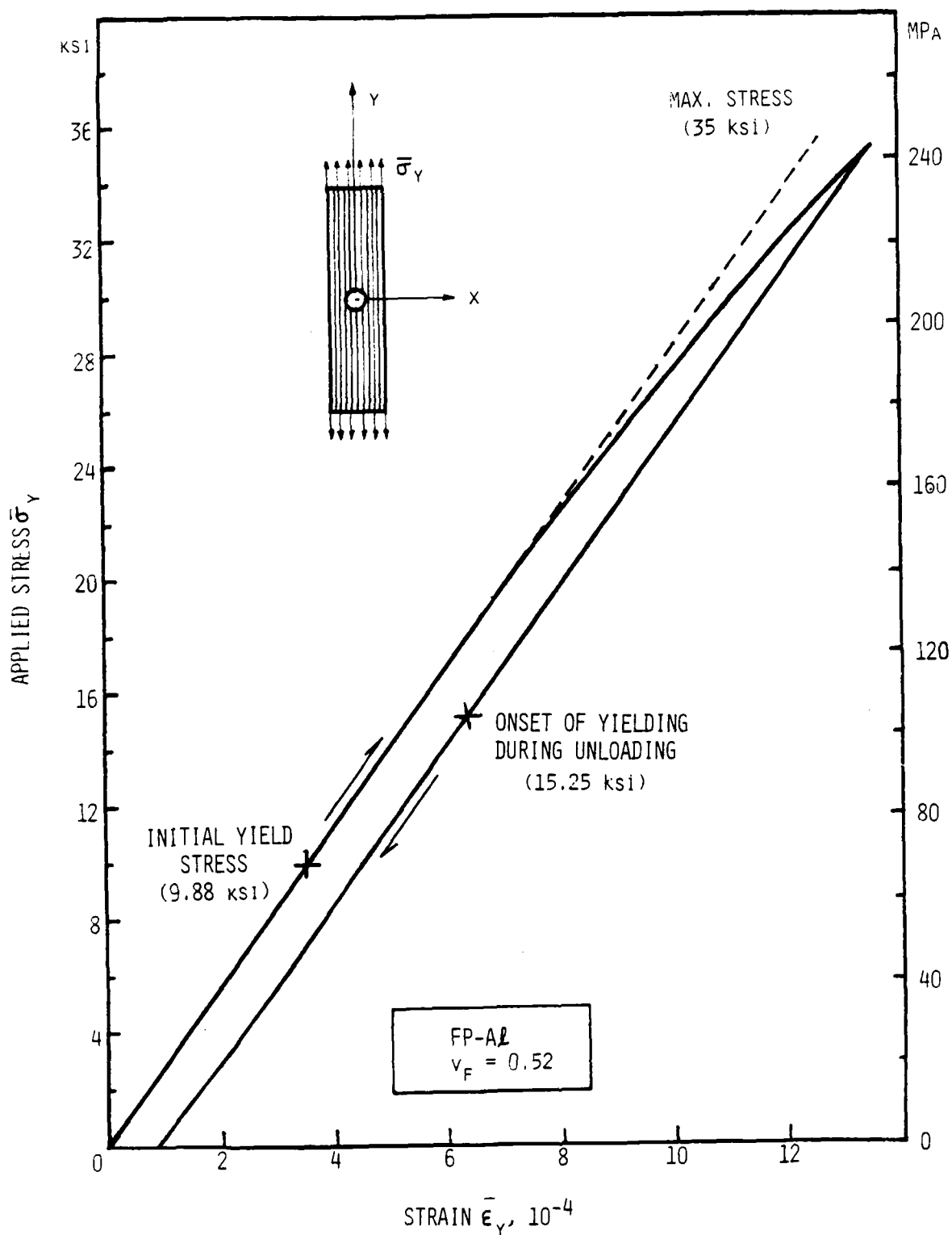
Figure 30. Calculated overall stress-strain response of the specimen with a circular hole
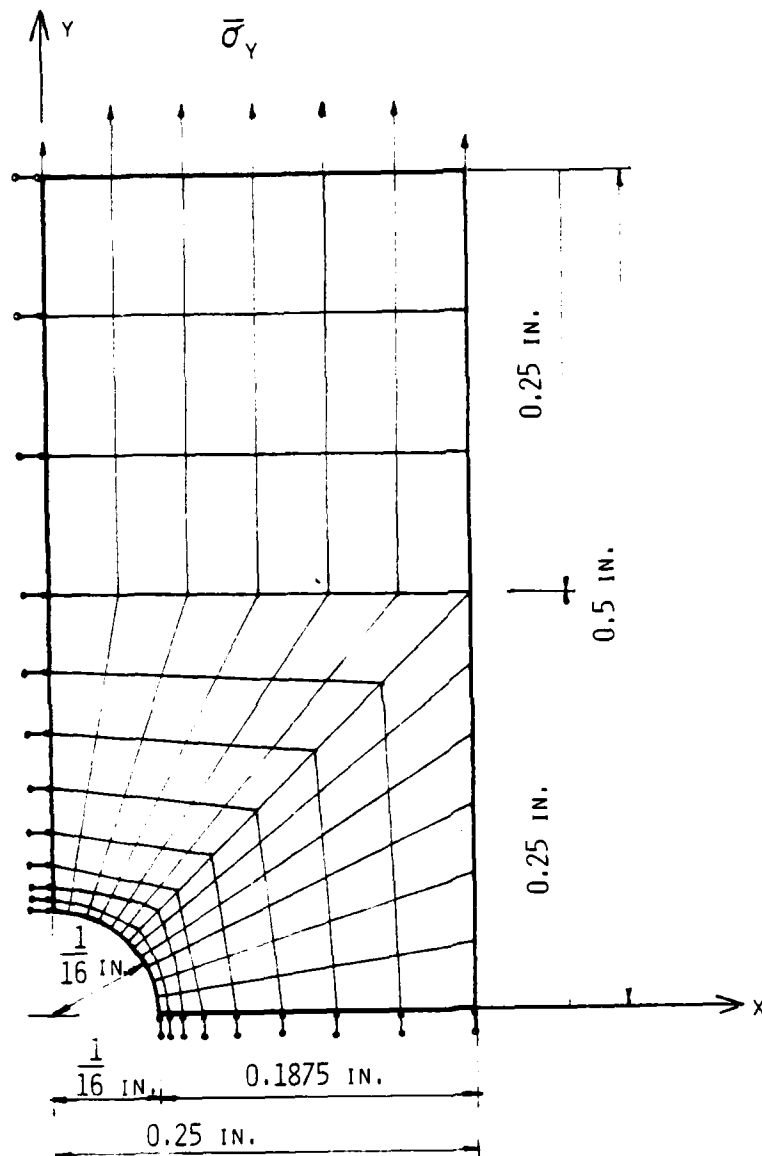
Figure 29. A finite element mesh used in plasticity analysis of the unidirectionally reinforced specimen with a drilled hole
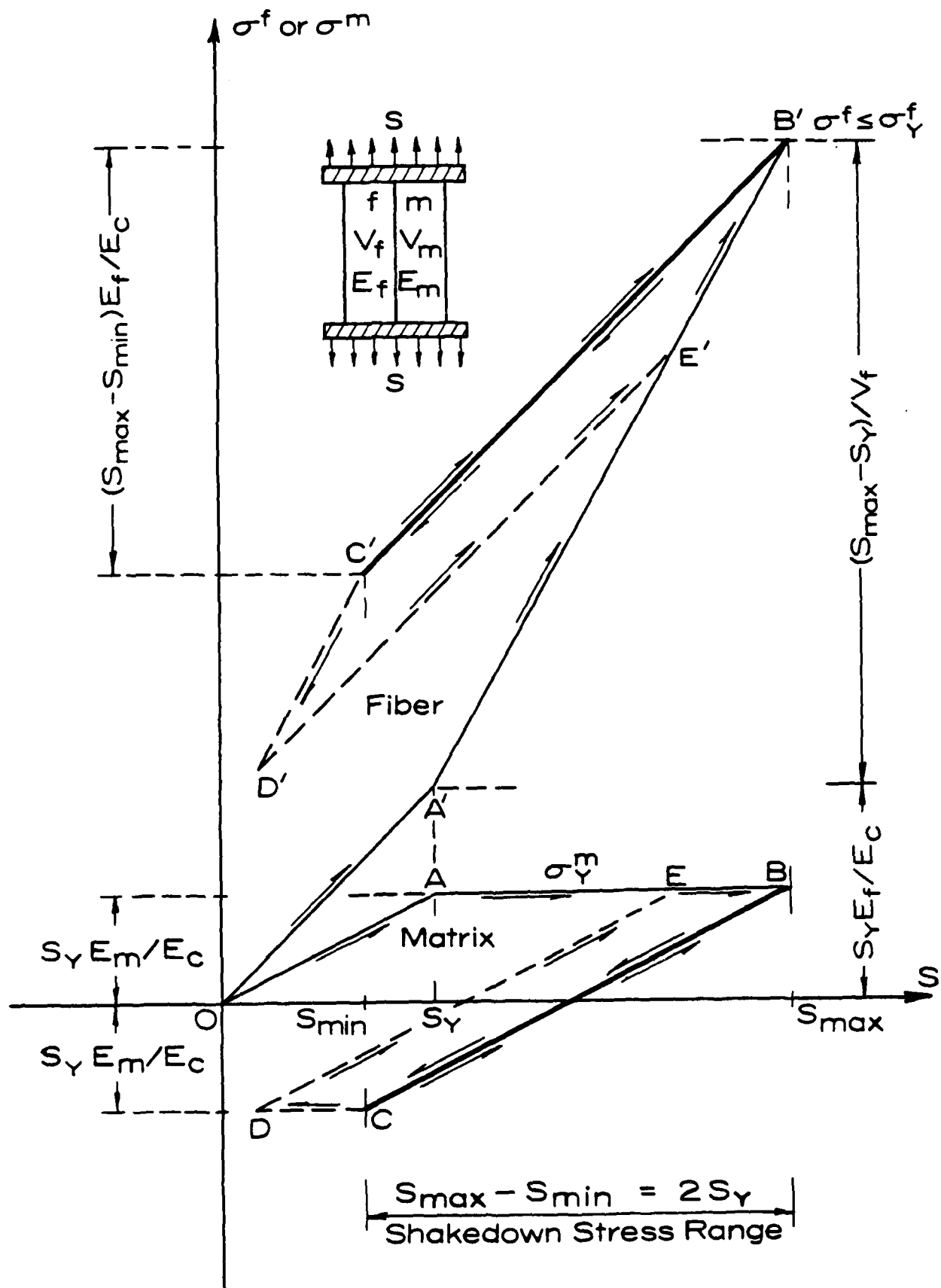
Figure 28. Schematic distribution of microstresses in fiber and matrix in an axially loaded unidirectional composite with a nonhardening matrix (From Dvorak and Tarn 1975)
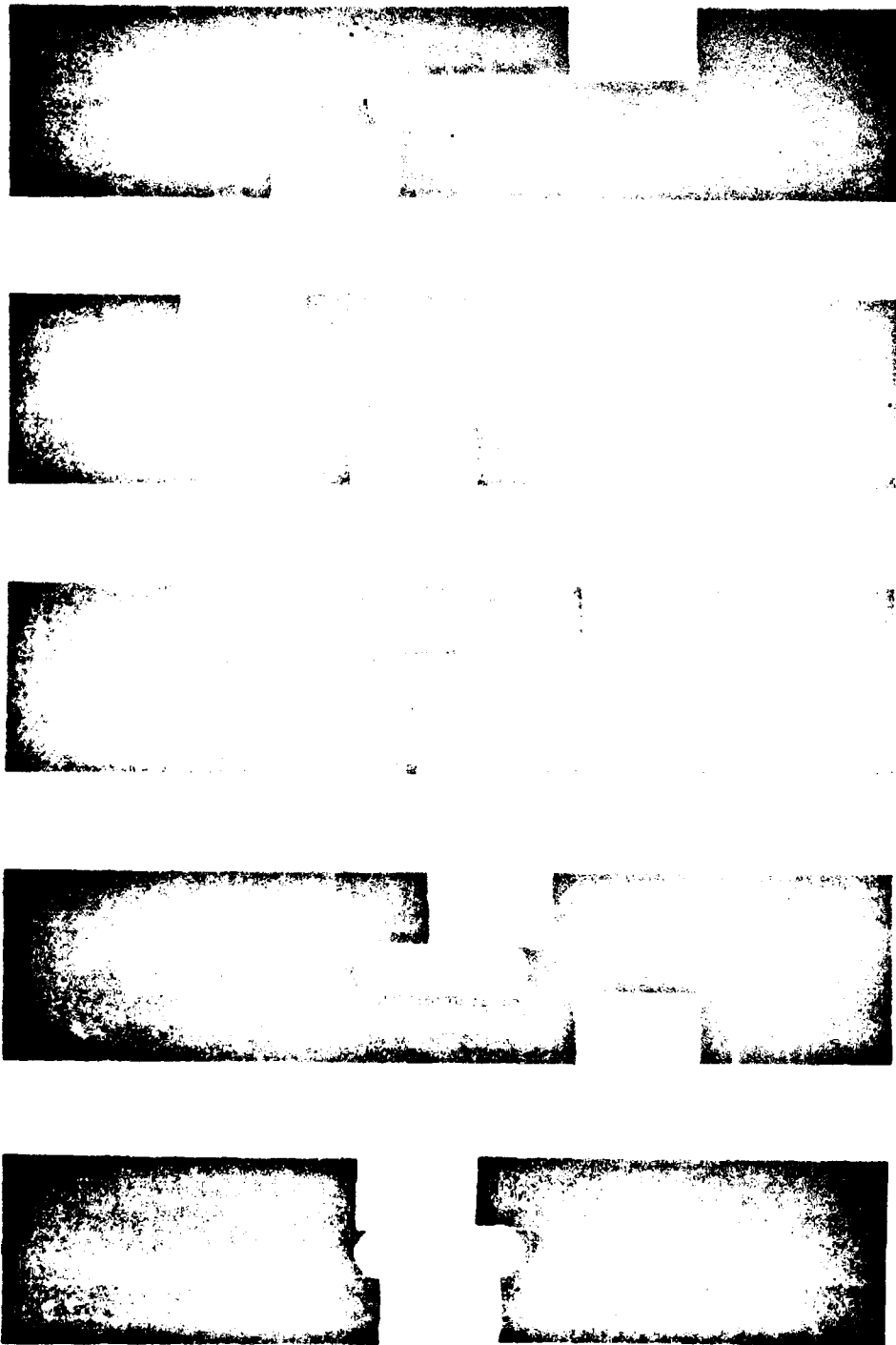
Figure 27.   Radiograph of broken test specimens with 3/8 in. hole from
             Figure 25, R = -1
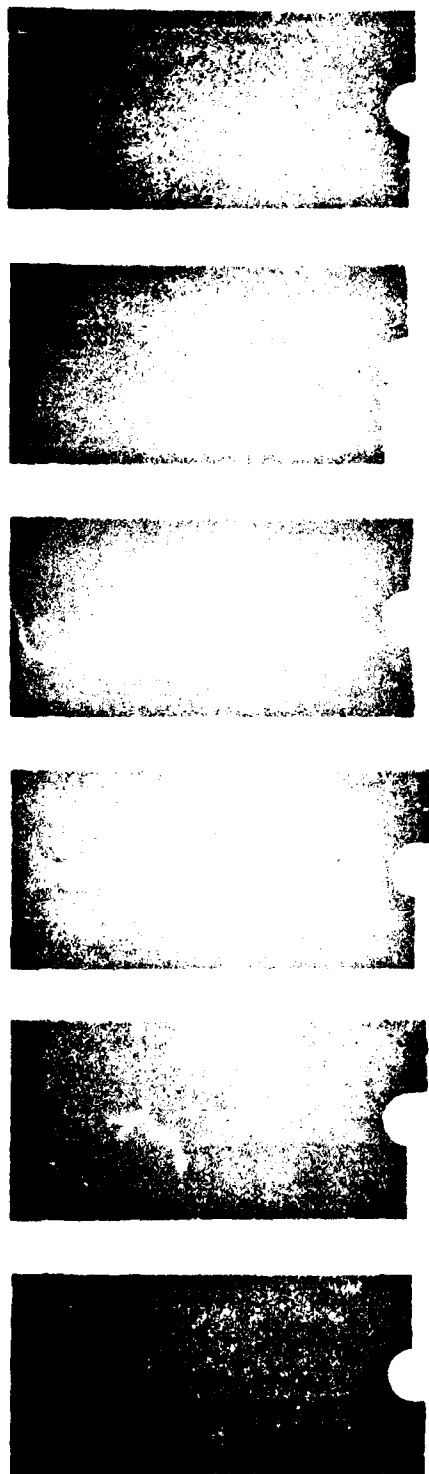
Figure 26. Radiographs of broken test specimens with 3/8 in. hole from Figure 23, R = 0.1
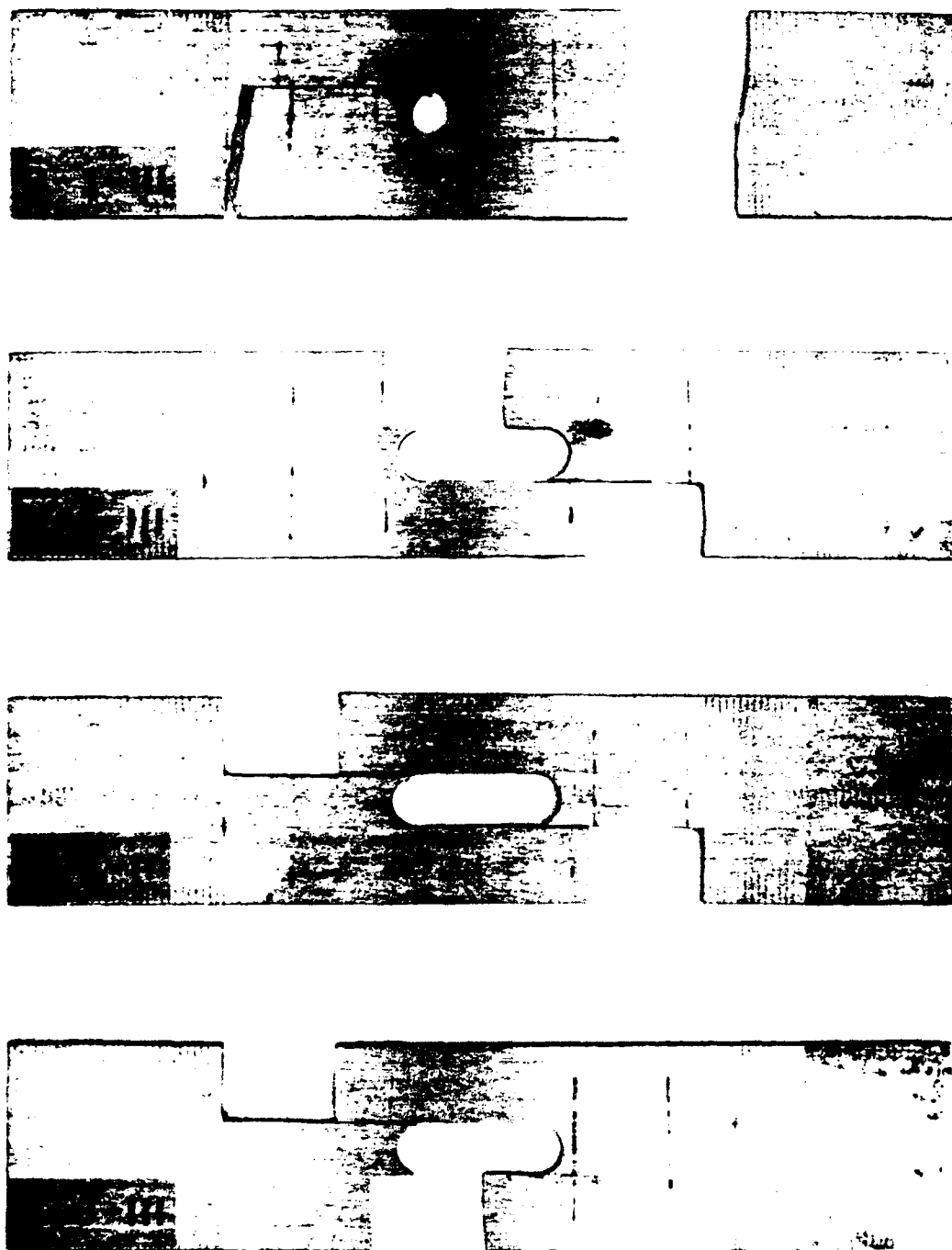
Figure 25. Broken test specimens with 3/8 in. hole, R = -1
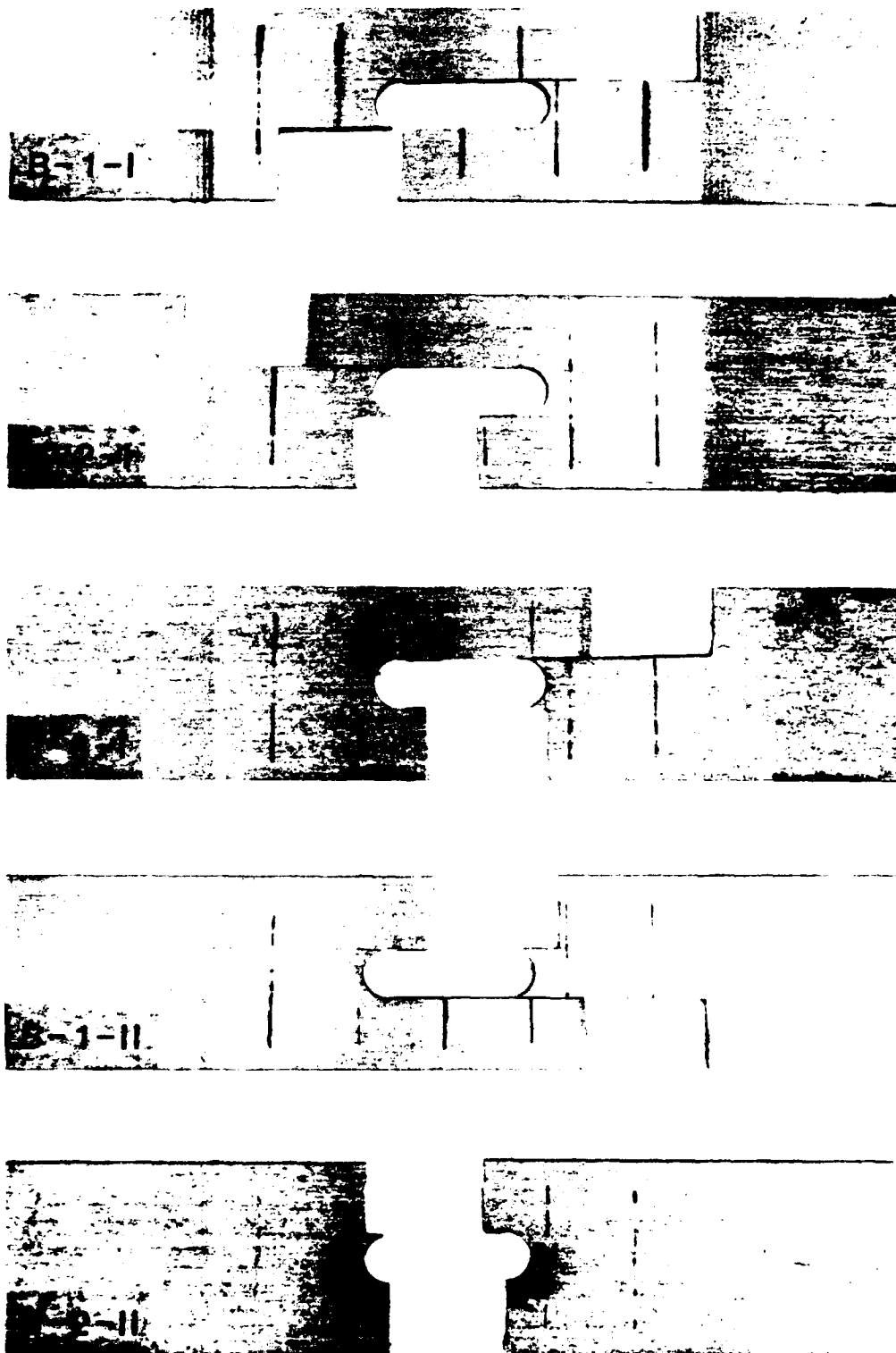
Figure 24.   Broken test specimens with 3/8 in. hole, R = -1

B-13-III

B-13-IV

B-14-IV

B-15-III

B-15-IV

B-27-II
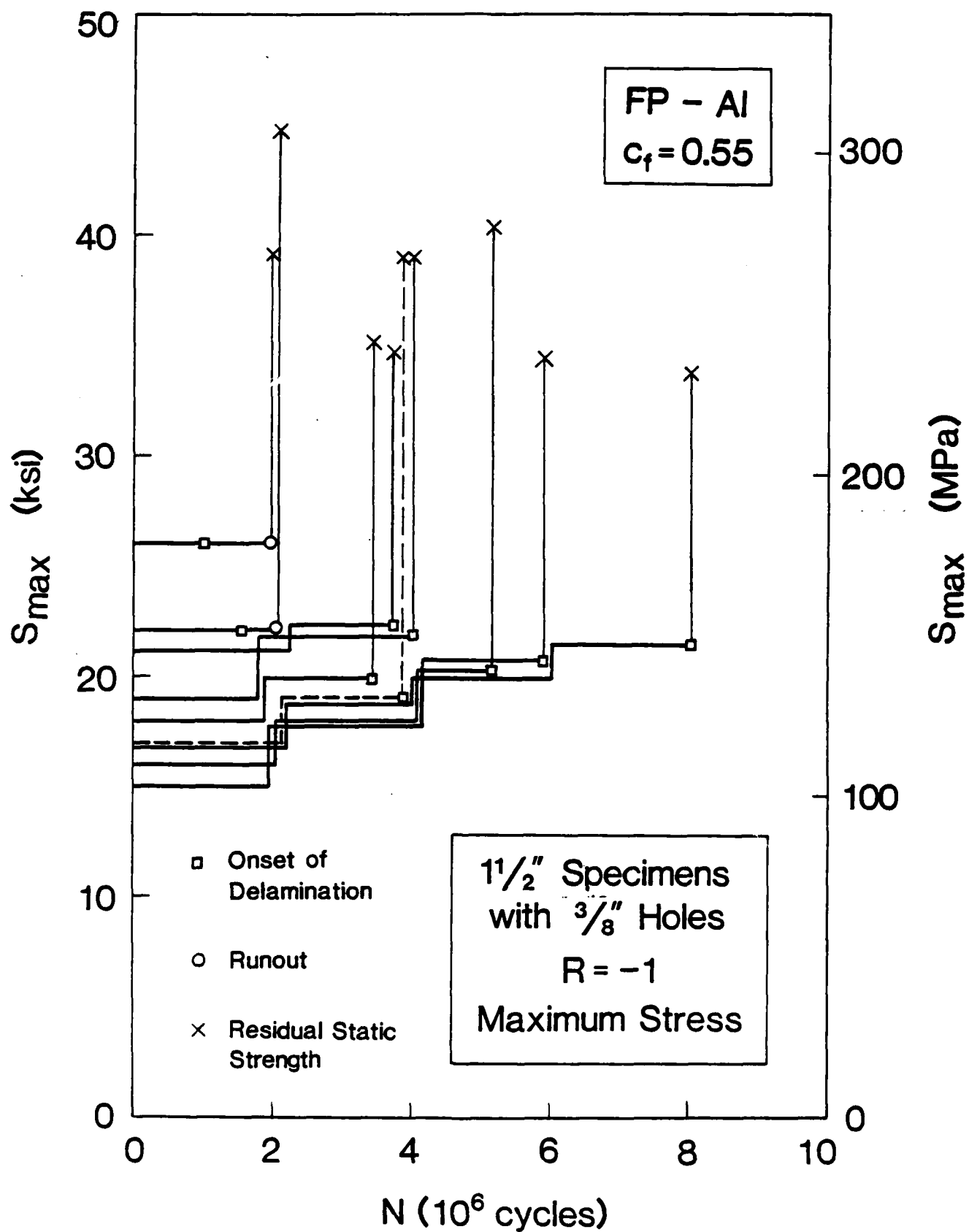
Figure 25.

Figure 22. Fatigue test results for 1 1/2 in. coupons with 3/8 in. drilled holes, R = -1
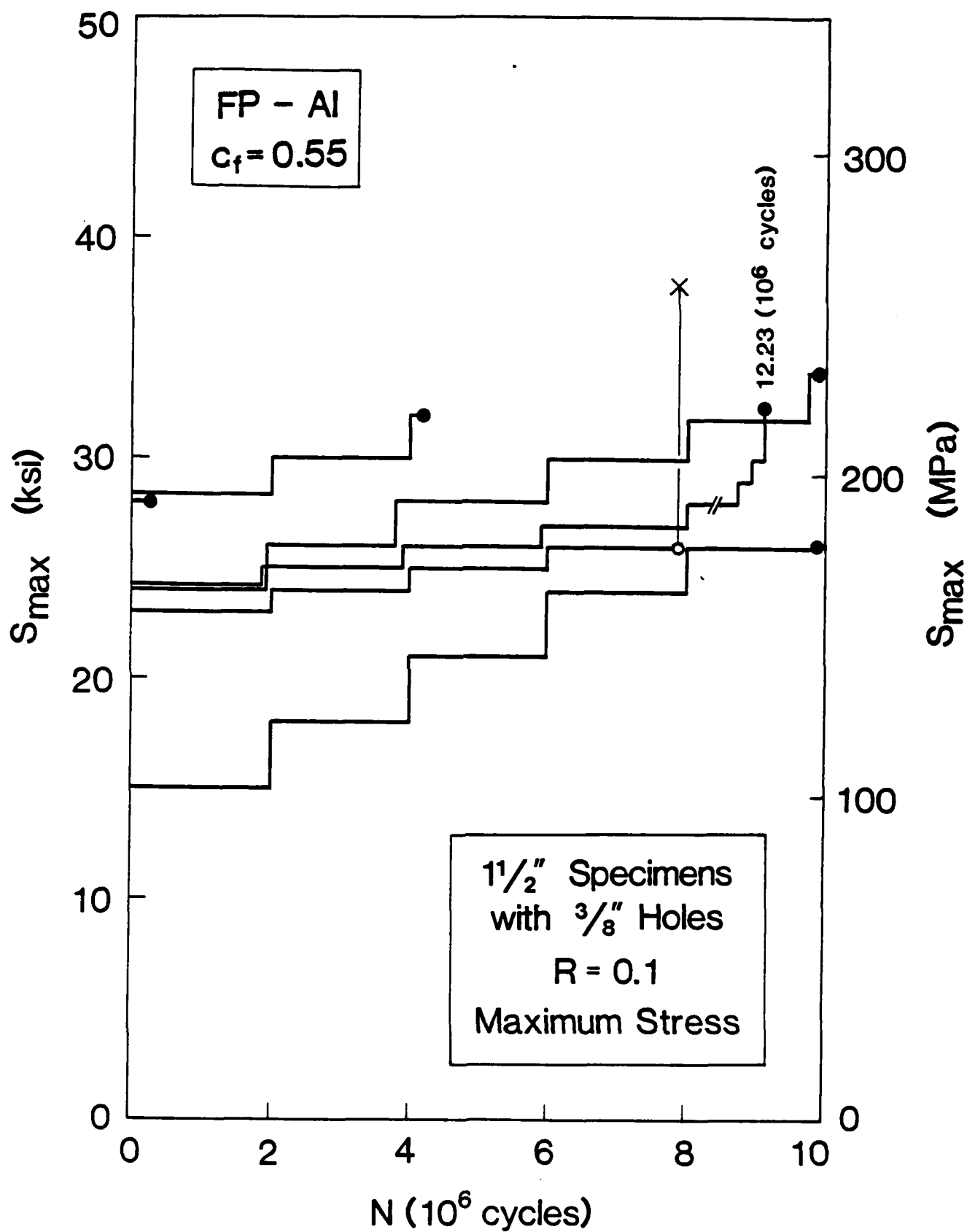
Figure 21.   Fatigue test results for 1 1/2 in. coupons with 3/8 in. drilled holes, R = 0.1
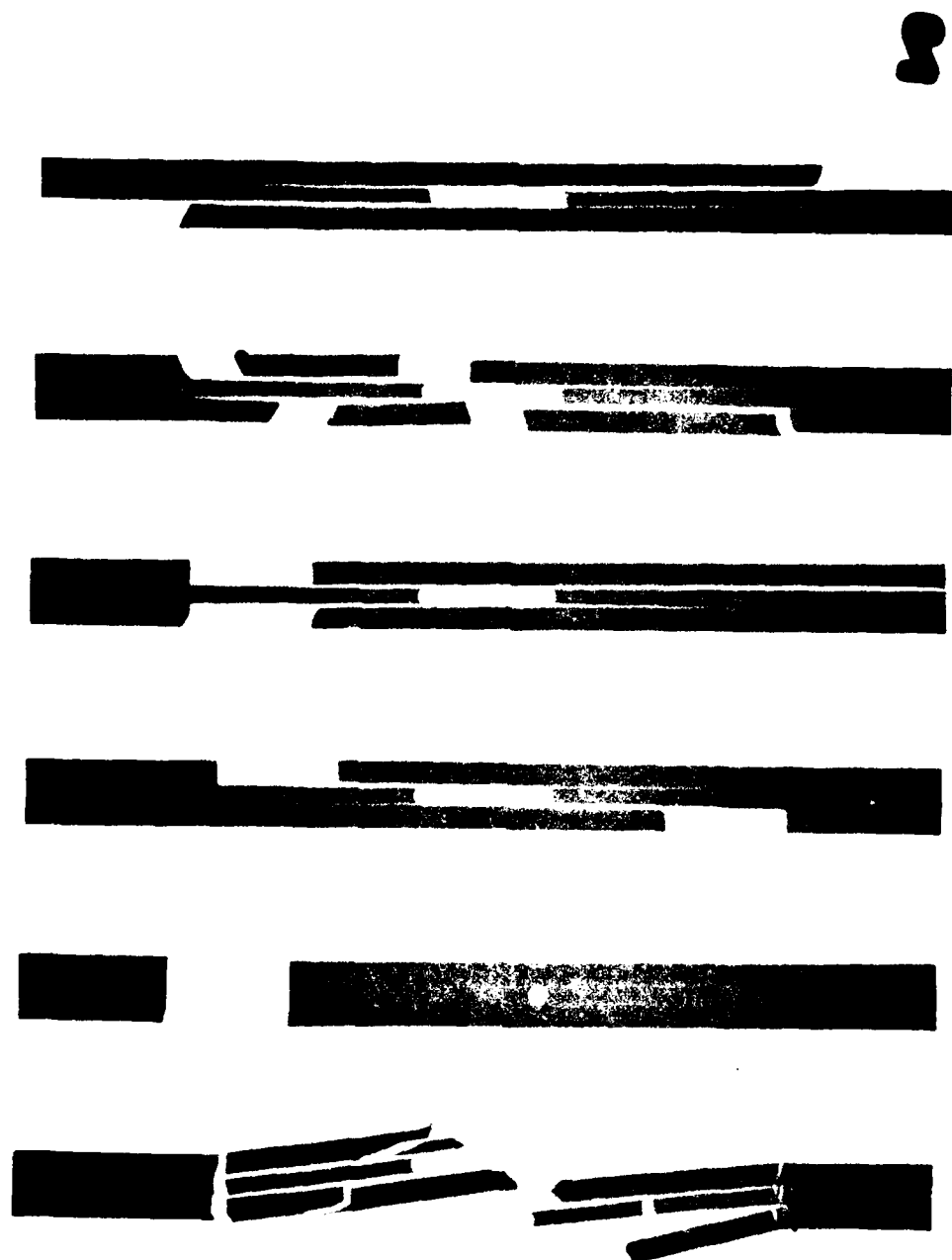
Figure 20. Radiographs of test specimens with 1/8 in. hole, R = -5
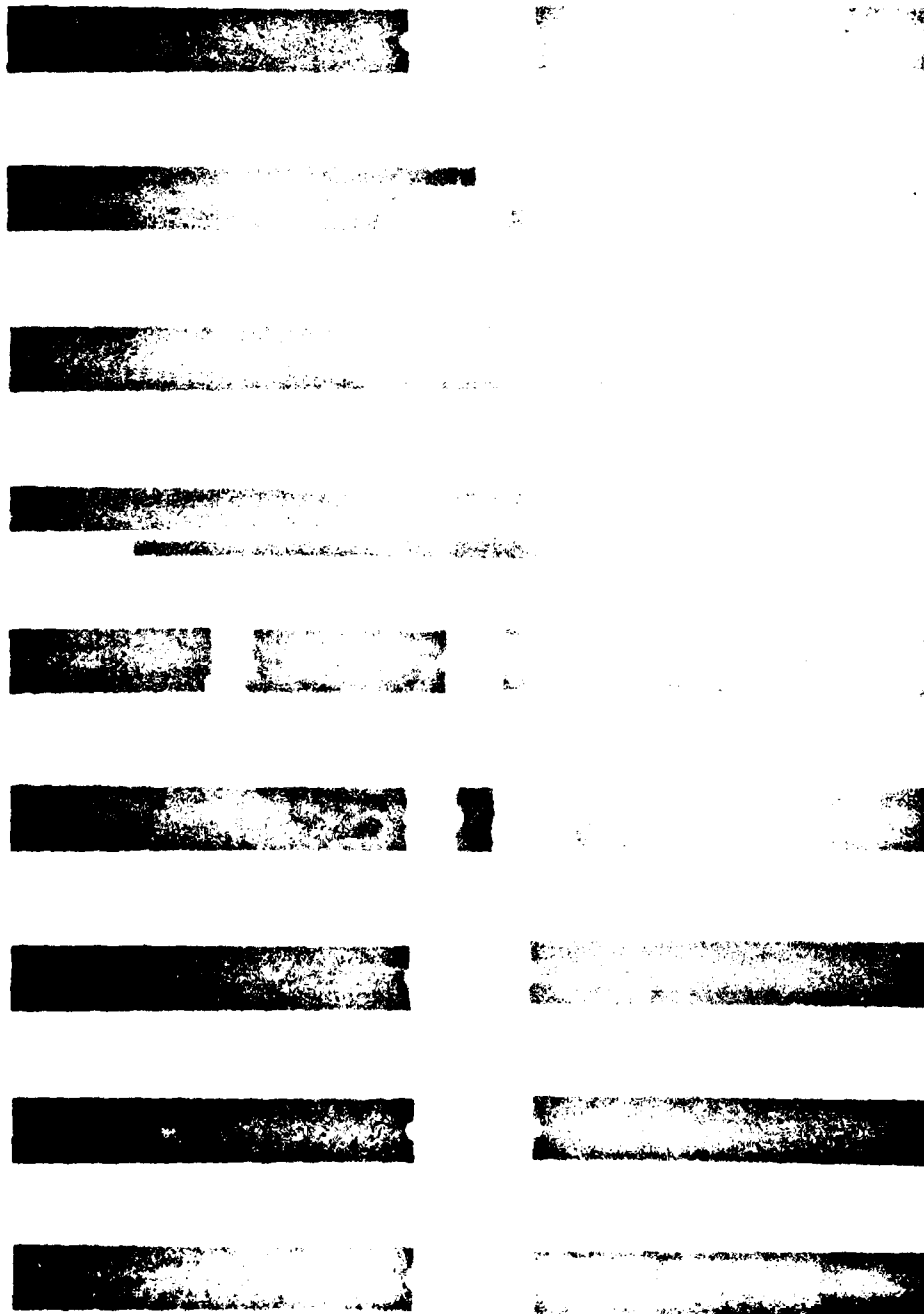
Figure 19. Radiographs of test specimens with 1/8 in. hole, R = -1 and static compression tests
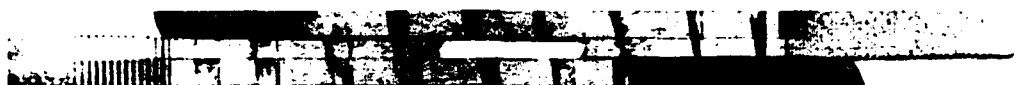
83-FP-2
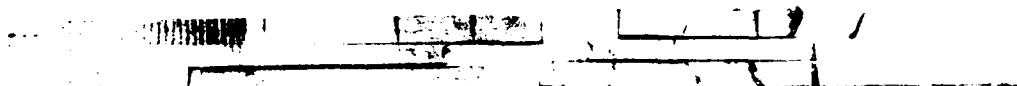
83-FP-6

83-FP-26
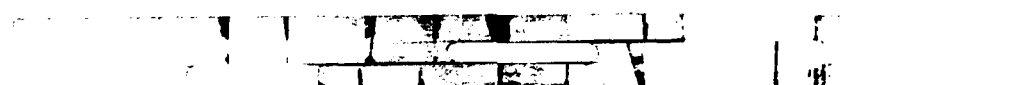
83-FP-33
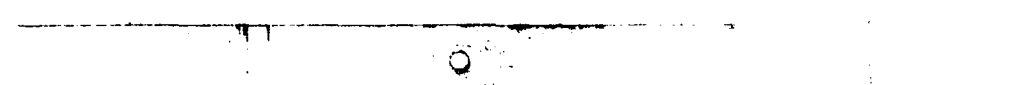
83-FP-35
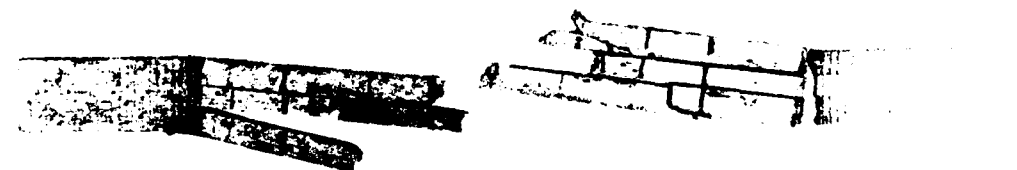
83-FP-39

Figure 18.   Broken test specimens with 1/8 in. hole, R = -5
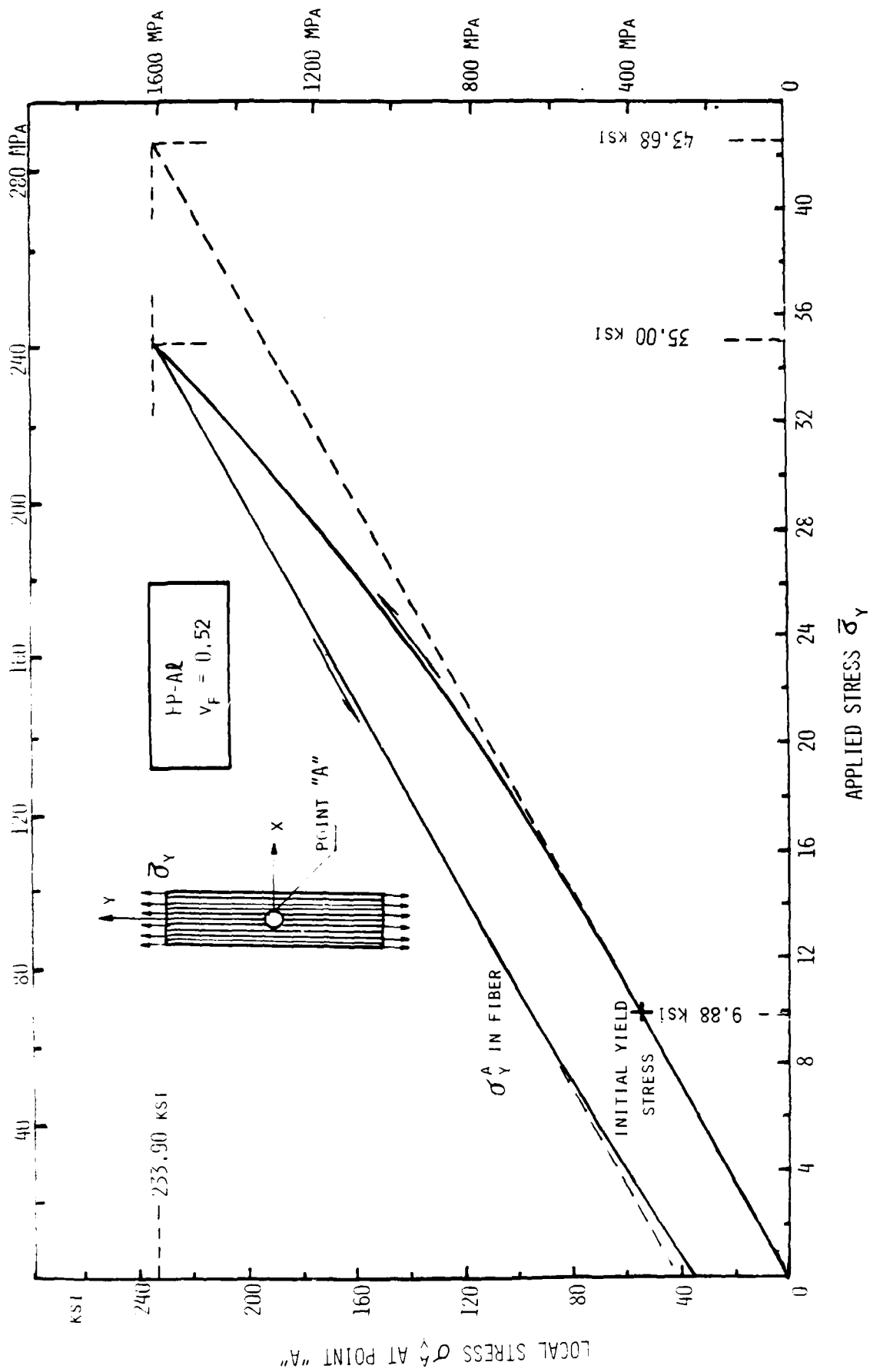
Figure 32. Fiber stress at the boundary of the circular hole during a load cycle

HOLE
DIAMETER

$\frac{1}{8}$ in.

$\frac{3}{8}$ in.

RESIDUAL TENSILE STRENGTH
242 – 248 MPa

300 ┬ MPa

200 —

100 —

0

-100 —

-200 —

-300 ┴

FP – Al
$C_f = 0.55$

$R = S_{min}/S_{max}$

1.0   0.1

-1.0 -2.0 -3.0 -4.0 -5.0

SHAKEDOWN
RANGE
150 MPa

STATIC AND RESIDUAL
COMPRESSIVE STRENGTH: –1310 MPa
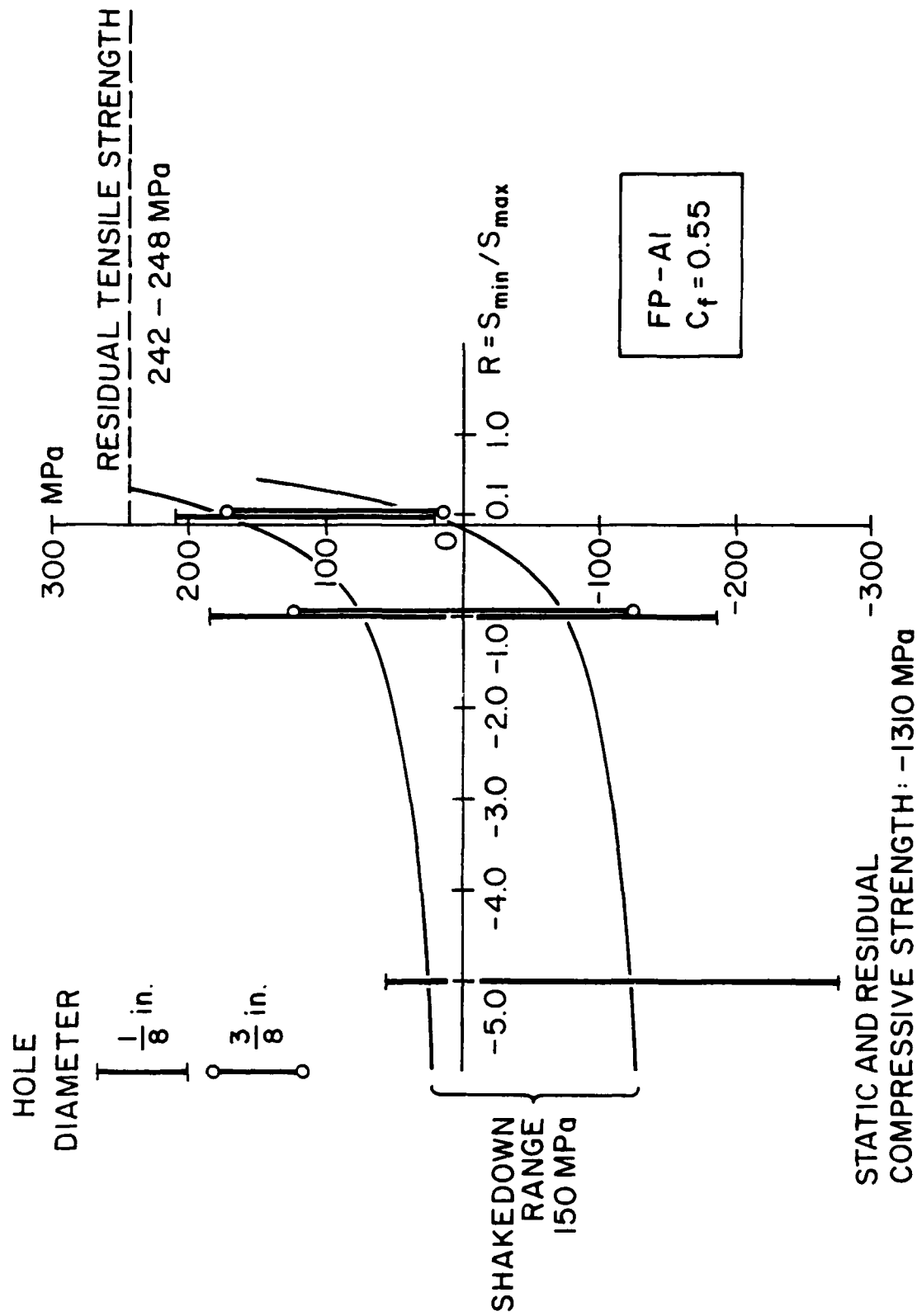
Figure 33. Endurance stress ranges of specimens with 1/8 in. and 3/8 in.
diameter holes. The shakedown range is shown for comparison
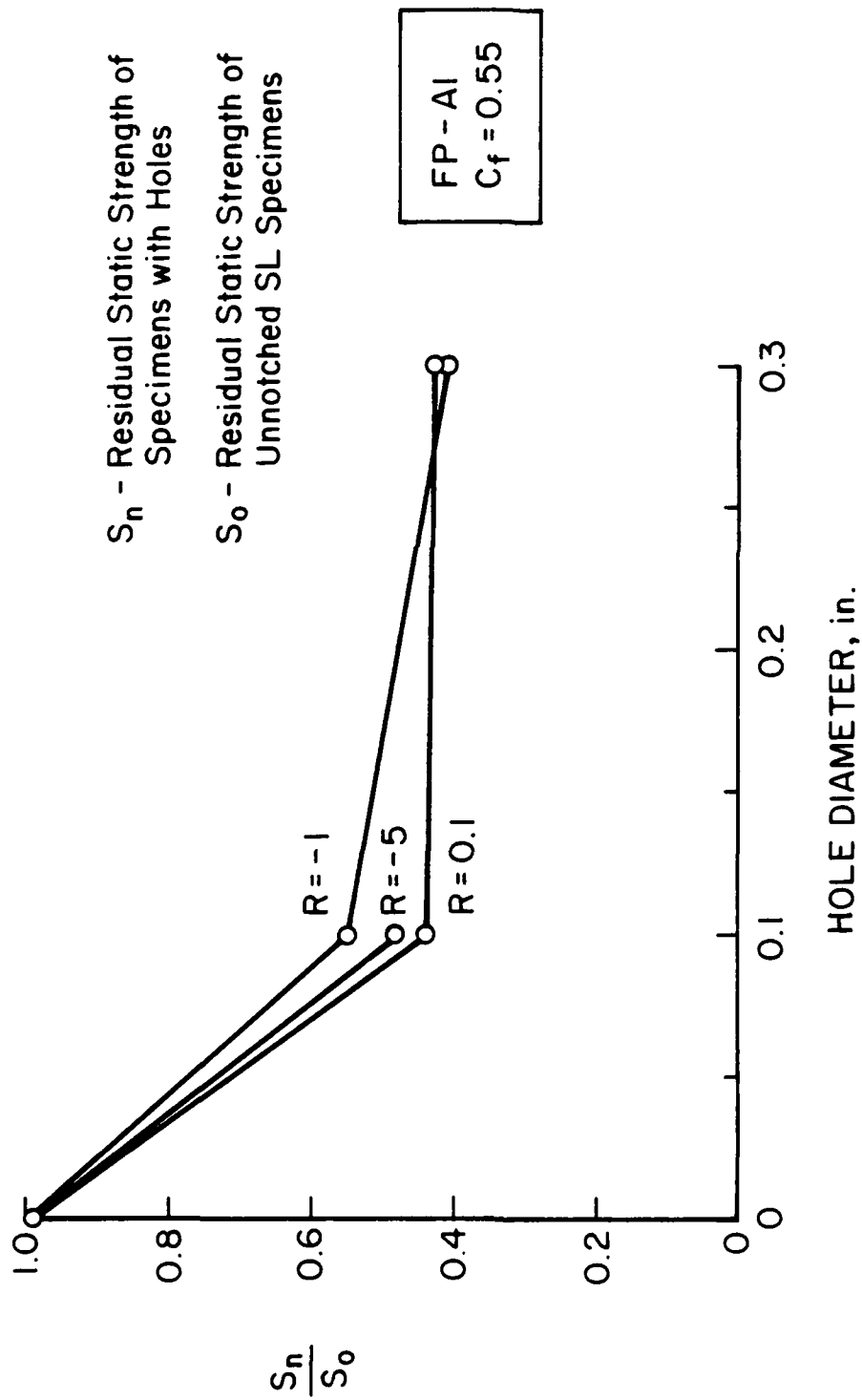
Figure 34. Reduction of residual static strength caused by variations in hole diameter and in cyclic stress ratio $R = S_{min}/S_{max}$
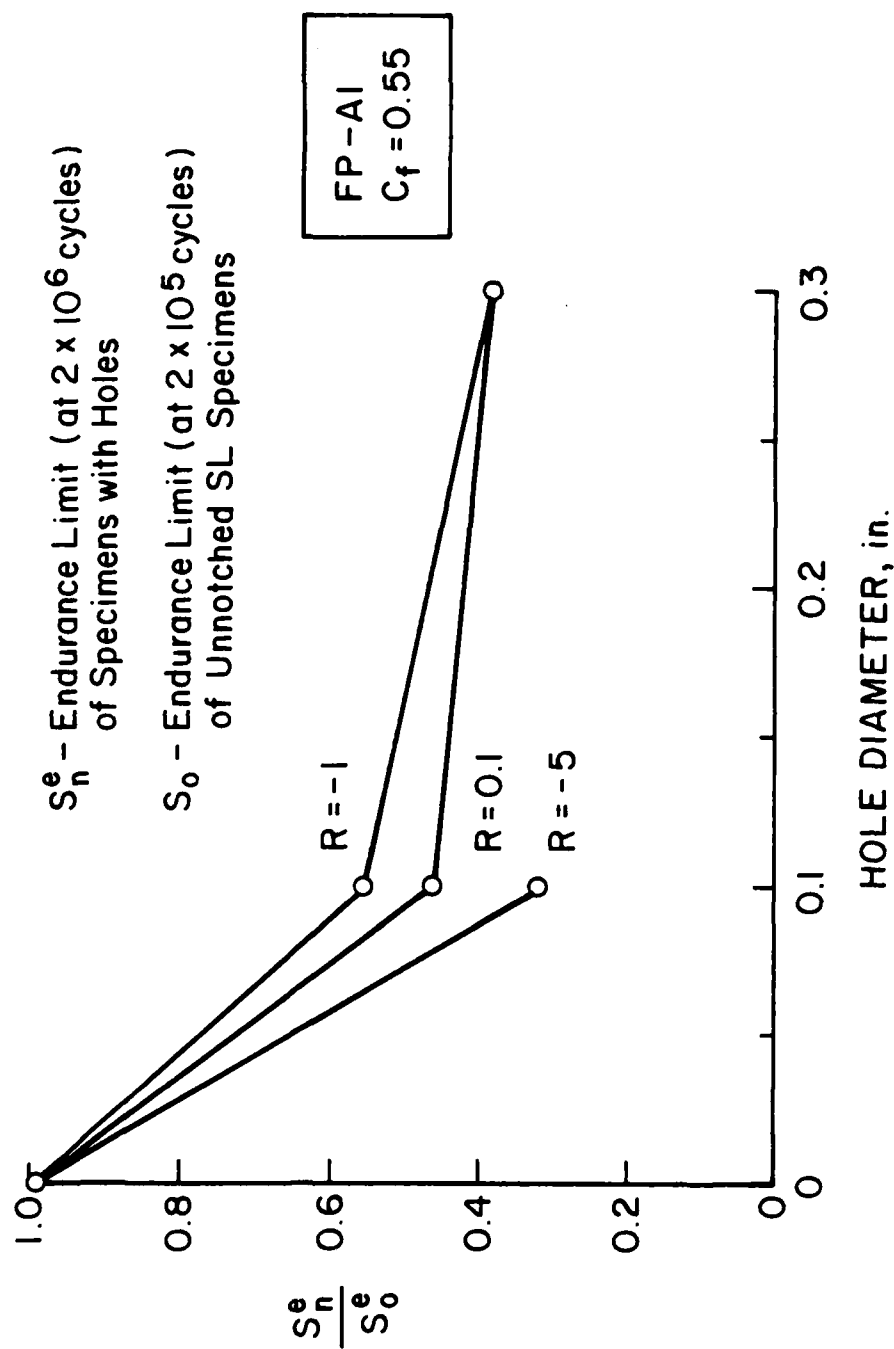
Figure 35. Reduction of endurance limits caused by variations in hole diameter and in cyclic stress ratio $R = S_{min}/S_{max}$

DISTRIBUTION LIST

No. of Copies	To
1	Office of the Under Secretary of Defense for Research and Engineering, The Pentagon, Washington, DC 20301
2	Commander, Defense Technical Information Center, Cameron Station, Building 5, 5010 Duke Street, Alexandria, VA 22314

Metals and Ceramics Information Center, Battelle Columbus Laboratories,
505 King Avenue, Columbus, OH 43201
1 ATTN: Mr. Robert J. Fiorentino, Program Manager

Defense Advanced Research Projects Agency, Defense Sciences Office/MSD,
1400 Boulevard, Arlington, VA 22209
1 ATTN: P. A. Parrish

Headquarters, Department of the Army, Washington, DC 20314
1 ATTN: DAEN-RDM, Mr. J. J. Healy

Deputy Chief of Staff for Research, Development and Acquisition,
Headquarters, Department of the Army, Washington, DC 20301
1 ATTN: DAMA-ARZ

Commander, U.S. Air Force Wright Aeronautical Laboratories,
Wright-Patterson Air Force Base, OH 45433
1 ATTN: AFWAL/FIBEC, Dr. Steve Johnson

Commander, Army Research Office, P.O. Box 12211, Research Triangle Park,
NC 27709
1 ATTN: Dr. George Mayer
1   Information Processing Office

Commander, U.S. Army Materiel Command, 5001 Eisenhower Avenue,
Alexandria, VA 22333
1 ATTN: AMCLD

Commander, U.S. Army Armament, Munitions and Chemical Command,
Dover, NJ 07801
1 ATTN: AMCAR-SCM, J. D. Corrie
1   Mr. Harry E. Pebly, Jr., PLASTEC, Director

Commander, U.S. Army Aviation Systems Command, 4300 Goodfellow Blvd.,
St. Louis, MO 63120
1 ATTN: AMCAV-NS, Harold Law

Chief of Naval Research, Arlington, VA 22217
1 ATTN: Dr. Steven G. Fishman

Naval Surface Weapons Center, White Oak, Silver Spring, MD 20910
1 ATTN: John V. Foltz - Code R32

No. of Copies	To
1	Mr. Leonard Poveromo, Grumman Aerospace Corp., Mail Stop A04-12, Bethpage, NY 11714
1	Mr. Steve Keck, RCA Astroelectronics, Mail Stop TR6B, P.O. Box 800, Princeton, NJ 08540

Director, Army Materials and Mechanics Research Center,
Watertown, MA 02172-0001

2	ATTN: AMXMR-PL
1	AMXMR-PR
1	AMXMR-K
10	AMXMR-SM, Dr. J. Slepetz

Army Materials and Mechanics Research Center
ATTN: AMXMR-K
Watertown, Massachusetts 02172-0001
FATIGUE BEHAVIOR OF UNIDIRECTIONAL
FP-Al COMPOSITE SPECIMENS WITH
CIRCULAR HOLES
George J. Dvorak
Department of Civil Engineering
Rensselaer Polytechnic Institute
Troy, NY 12180

Technical Report AMMRC TR 88-44, November 1984
Illus.-tables, Contract DAAG46-80-C-0059
D/A Project: 1L162105AHR4
Final Report, July 80 to July 83

Fatigue behavior of two different batches of fibrous FP-Al composites was investigated. The nominal fiber volume fraction of the two batches was 0.52 and 0.55, respectively. Several specimen types were tested: the unnotched coupon, the SL specimen, and two types of coupons with 1/8 in. and 3/8 in. diameter circular holes. One group of unnotched coupons was reinforced in the transverse direction, all other specimens were reinforced in the direction of the applied load. Cyclic loading was applied at constant amplitude, at three different cyclic ratios R = Smin/Smax, equal to 0.1, -1.0, and -5.0. Fatigue endurance limits are significantly smaller than the residual static strength, especially at R = -1.0, and R = -5.0. The strength reduction is particularly pronounced in compression. The unidirectional FP-Al material delaminates rather easily under compression loading, and this reduces its compression endurance limit to values which can be as low as 18% of the static compression strength.

END

FILMED

6-85

DTIC